JOURNAL OF PETROLOGY | VOLUME 52 | NUMBER 12 | PAGES 2397–2429 | 2011 | doi:10.1093/petrology/egr050

Isotopic Evolution of the Idaho Batholith and Challis Intrusive Province, Northern US Cordillera

RICHARD M. GASCHNIG[1]*, JEFFREY D. VERVOORT[1], REED S. LEWIS[2] AND BASIL TIKOFF[3]

[1]SCHOOL OF EARTH AND ENVIRONMENTAL SCIENCES, WASHINGTON STATE UNIVERSITY, PULLMAN, WA 99164, USA

[2]IDAHO GEOLOGICAL SURVEY, UNIVERSITY OF IDAHO, MOSCOW, ID 83844, USA

[3]DEPARTMENT OF GEOSCIENCE, UNIVERSITY OF WISCONSIN-MADISON, MADISON, WI 53706, USA

RECEIVED SEPTEMBER 20, 2010; ACCEPTED SEPTEMBER 28, 2011

The Idaho batholith and spatially overlapping Challis intrusive province in the North American Cordillera have a history of magmatism spanning some 55 Myr. New isotopic data from the ~98 Ma to 54 Ma Idaho batholith and ~51 Ma to 43 Ma Challis intrusions, coupled with recent geochronological work, provide insights into the evolution of magmatism in the Idaho segment of the Cordillera. Nd and Hf isotopes show clear shifts towards more evolved compositions through the batholith's history and Pb isotopes define distinct fields correlative with the different age and compositionally defined suites of the batholith, whereas the Sr isotopic compositions of the various suites largely overlap. The subsequent Challis magmatism shows the full range of isotopic compositions seen in the batholith. These data suggest that the early suites of metaluminous magmatism (98–87 Ma) represent crust–mantle hybrids. Subsequent voluminous Atlanta peraluminous suite magmatism (83–67 Ma) results primarily from melting of different crustal components. This can be attributed to crustal thickening, resulting from either subduction processes or an outboard terrane collision. A later, smaller crustal melting episode, in the northern Idaho batholith, resulted in the Bitterroot peraluminous suite (66–54 Ma) and tapped different crustal sources. Subsequent Challis magmatism was derived from both crust and mantle sources and corresponds to extensional collapse of the over-thickened crust.

KEY WORDS: *Idaho batholith; radiogenic isotopes; North American Cordillera; granite; zircon; Pb isotopes; Lu–Hf; Sm–Nd; Sr isotopes*

INTRODUCTION

The issues of how continental crust forms and how rates of crustal production have changed through the Earth's history remain fundamental, first-order questions in geology. In the context of continental arcs, it is not well understood, for example, to what extent they are produced by juvenile contributions from the mantle or by melting of existing arc crust, how these contributions vary throughout the lifetime of arcs, and the role tectonics plays in moderating the two processes (e.g. Gromet & Silver, 1987; Ellam & Hawkesworth, 1988; Rudnick, 1995; Petford & Atherton, 1996; Coleman & Glazner, 1997; Ducea, 2001; Saleeby *et al.*, 2003; Davidson & Arculus, 2005; Ducea & Barton, 2007; Lee *et al.*, 2007; Kemp *et al.*, 2009). The Cordilleran batholiths of North America have long been a major focus of these inquiries, and recent work suggests that magmatic flux and composition are driven by tectonic cycling (Ducea & Barton, 2007; DeCelles *et al.*, 2009).

The Idaho batholith represents a unique segment of the Cordilleran arc that is currently poorly understood. The batholith and the subsequent, but spatially overlapping, Challis magmatic province are emplaced entirely in ancient Precambrian crust and are dominated by evolved peraluminous compositions. In contrast, the other Cordilleran batholiths intrude accreted oceanic terranes

Corresponding author. Present address: Department of Geology, University of Maryland, College Park, MD 20742, USA. E-mail: gaschnig@umd.edu

or transitional crust and typically consist of less evolved hornblende-bearing granodiorites, tonalites, and quartz diorites (e.g. Todd & Shaw, 1985; Armstrong, 1988; Bateman, 1992; Friedman *et al.*, 1995). For the Idaho batholith, the distinct isotopic compositions of the Precambrian crust provide leverage to better determine the relative roles of crustal growth and recycling, which are more ambiguous for other Cordilleran batholiths owing to the young and isotopically juvenile nature of the crust they intrude. In addition, recent advances in our understanding of the chronology of magmatism in the Idaho batholith and Challis systems (e.g. Gaschnig *et al.*, 2010, and references therein) provide a unique opportunity to track temporal changes in magma chemistry and the evolution of the magma sources. Understanding how these different sources combine through time, in turn, provides insights into the link between magmatism and tectonics.

In this study, we use multiple radiogenic isotope systems to show that the magmatism was initially similar to that of the other Cordilleran arcs, dominated by mixing of melts from crust and mantle sources. Progressive crustal thickening caused a shift from metaluminous to peraluminous magmatism, produced by melting of dominantly crustal sources, in two major episodes. Ultimately, extensional collapse of the over-thickened Cordilleran arc crust led to increased inputs of magma from the mantle and a renewal of crust–mantle hybridization, leading to the Challis intrusive province and coeval volcanic field.

GEOLOGIC BACKGROUND

The Idaho batholith (Fig. 1) is fundamentally different from the other major batholiths of the North American Cordillera. It is dominated by peraluminous granites, and emplaced entirely in Precambrian continental crust (e.g. Armstrong *et al.*, 1977; Hyndman, 1983). In contrast, the other Cordilleran batholiths are characterized by metaluminous compositions and are emplaced mostly in accreted juvenile crust. The Idaho batholith was emplaced primarily into Mesoproterozoic (Belt Supergroup; Hyndman, 1983) and Neoproterozoic (Windermere Supergroup; Lund *et al.*, 2003, 2008) metasedimentary rocks. The nature of the underlying crystalline basement is poorly understood and has been described as a Paleoproterozoic composite terrane [termed Wallace by Sims *et al.* (2005) and Selway by Foster *et al.* (2006)]. Foster *et al.* (2006) defined it as a collage of arc-like terranes ranging in age from 2·4 to 1·6 Ga. More recently, new exposures of *c.* 2·66 and 1·86 Ga meta-igneous basement have been identified just north of the Idaho batholith (Vervoort *et al.*, 2007; Brewer *et al.*, 2008). Archean crustal blocks are present to the south of the batholith, beneath the Snake River Plain (Leeman *et al.*, 1985; Wolf *et al.*, 2005), and to the north, exposed in the Priest River complex (Doughty *et al.*, 1998), but the exact locations of their boundaries are not well established.

The Idaho batholith (Fig. 1) is bordered to the west by a major lithospheric-scale structure termed the Salmon River suture zone. This structure separates Precambrian North American crust to the east from the Blue Mountains province, a collage of Late Paleozoic to Jurassic island arc terranes (Lund & Snee, 1988), to the west. The suture zone is characterized by a remarkably sharp isotopic transition unique in the Cordillera, reflecting the truncation of the Neoproterozoic–Paleozoic continental margin and near-vertical geometry of the structure (Armstrong *et al.*, 1977; Fleck & Criss, 1985, 2007; Manduca *et al.*, 1992). It was formed by the accretion of the Blue Mountains province in the early Cretaceous and was intruded by a group of small, compositionally diverse plutons between ~125 and ~90 Ma (Manduca *et al.*, 1993; Lee, 2004; Snee *et al.*, 2007; Schmidt *et al.*, 2009) that we term the suture zone suite. The suture zone was subsequently modified by dextral transpressional deformation in the middle to Late Cretaceous, which led to the formation of the discrete western Idaho shear zone within the suture (McClelland *et al.*, 2000; Giorgis *et al.*, 2008).

Units of the Idaho batholith and Challis intrusive province

The Idaho batholith (Fig. 1), in a broad sense, consists of a northern Bitterroot lobe and a larger, southern Atlanta lobe, both of which are dominated by peraluminous granites, in contrast to the other main Cordilleran batholiths (Hyndman, 1983). The Idaho batholith is also unusual in that it lacks the large discrete mappable plutons with distinct contacts that characterize the other Cordilleran batholiths. Based on bulk-rock lithology and age, we have identified five basic rock suites (Gaschnig *et al.*, 2010): the early metaluminous, border zone, Atlanta peraluminous, late metaluminous, and Bitterroot peraluminous suites.

The early metaluminous suite (98–87 Ma; Fig. 1) is the oldest component of the Idaho batholith. It consists of discrete metaluminous, hornblende-bearing plutons, typically containing mafic microgranular enclaves. These plutons occur as outlying stocks in the southeastern Atlanta lobe but trend to the NW and occur as roof pendants within the younger Atlanta peraluminous rocks to the north. The metaluminous suite includes a distinct subset of plutons containing poikilitic K-feldspar megacrysts up to 10 cm long. Screens of augen gneiss in the western and north–central Bitterroot lobe may represent deformed continuations of this unit (Lund *et al.*, 2008).

The border zone suite forms the western boundary of the Atlanta lobe and is immediately east of, and parallel to, the western Idaho shear zone. It formed primarily around 90 Ma and consists of tabular tonalite, granodiorite, and quartz diorite plutons, commonly with steeply dipping foliations. The Payette River tonalite, described in detail by

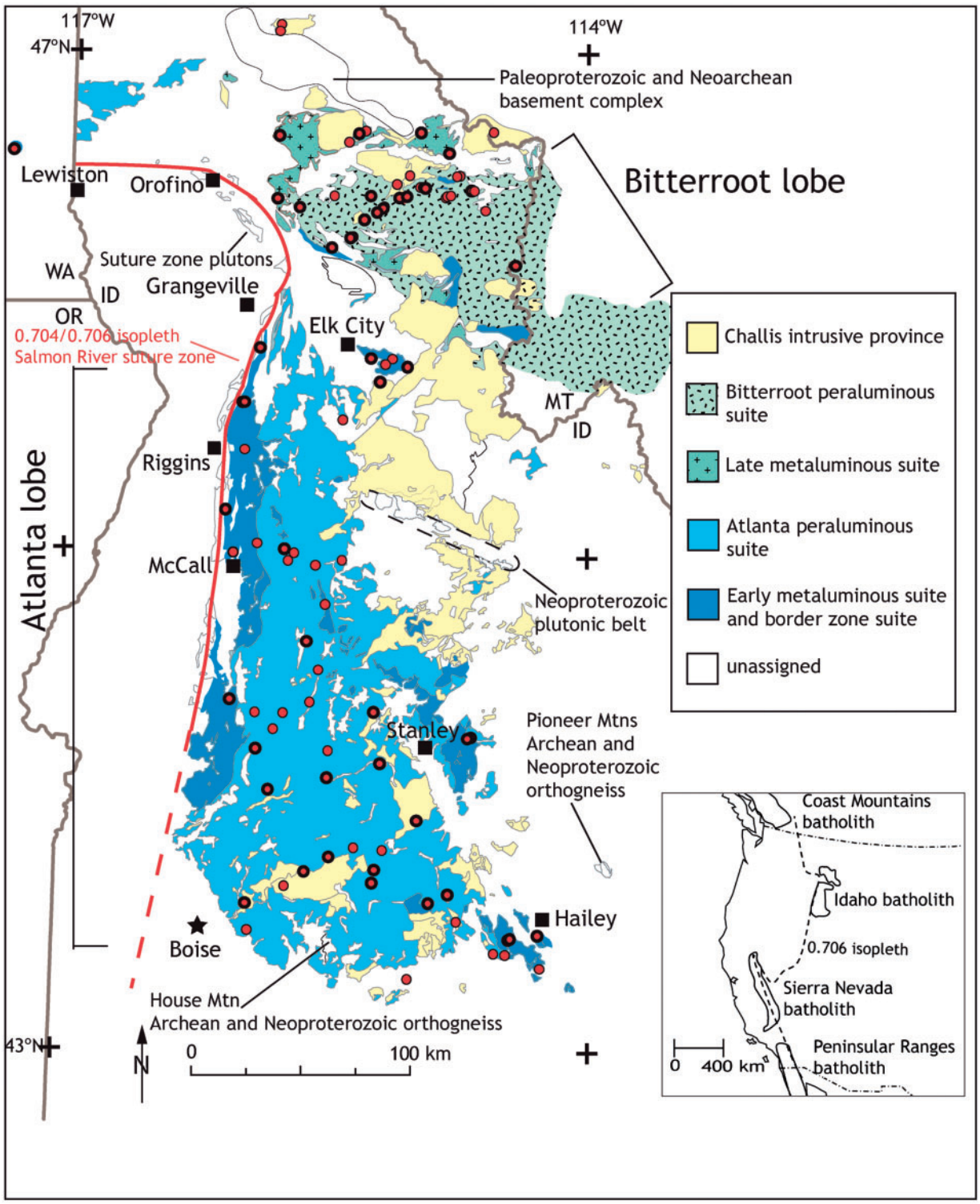

Fig. 1. Simplified geological map of the Idaho batholith showing the major lithological suites; modified from Gaschnig *et al.* (2010). Circles represent samples with data from this study. Circles outlined in black have been previously dated by U–Pb zircon methods (McClelland & Oldow, 2007; Murphy, 2007; Giorgis *et al.*, 2008; Lund *et al.*, 2008; Unruh *et al.*, 2008; Gaschnig *et al.*, 2010).

Manduca *et al.* (1992, 1993), is an example of this suite. The overlapping ages and compositions of the border zone and early metaluminous suite suggest a link that will be discussed below.

The Atlanta lobe is dominated by the Atlanta peraluminous suite (83–67 Ma). It consists of a relatively homogeneous biotite granodiorite, cored by bodies of muscovite–biotite granite or granodiorite and cut by dikes and small masses of biotite leucogranite. These units are weakly to strongly peraluminous, exhibit only limited geochemical and petrographic variation, and commonly are leucocratic (color index $\leq$5). Most of the muscovite in these compositions is thought to be magmatic based on textural criteria (Kiilsgaard & Lewis, 1985).

The Bitterroot lobe contains a small belt of fringing metaluminous plutons termed the late metaluminous suite (75–69 Ma). These plutons range in composition from quartz diorite to granodiorite. The majority of the Bitterroot lobe, however, consists of the Bitterroot peraluminous suite (66–53 Ma). It is dominated by biotite granodiorite similar petrographically and geochemically to the equivalent unit in the Atlanta lobe, despite being distinctly younger. Muscovite-bearing granite is less common and generally occurs in close proximity to metasedimentary wall-rocks. Outcrop-scale textural heterogeneities are more common than in the Atlanta peraluminous suite, and mafic dikes, sills, and small plutons are present, which we collectively refer to as the Bitterroot mafic rocks. Hyndman & Foster (1988) and Foster & Hyndman (1990) interpreted the mafic rocks to be comagmatic with the peraluminous suite, but there is evidence that some of the mafic rocks are Eocene in age and associated with the Challis intrusions (Gaschnig *et al.*, 2010).

All units of the Idaho batholith are cut by Eocene epizonal plutons and dikes associated with the Challis volcanic field in east–central Idaho. These are the Challis intrusions (51–44 Ma), and they are divided into a pink granite suite, which consists of granite (*senso stricto*) and syenite considered comparable to A-type granites (Lewis & Kiilsgaard, 1991), and a quartz monzodiorite suite consisting of diverse lithologies from gabbro to granite (Lewis & Kiilsgaard, 1991).

Previous work

The geochemistry and petrology of the Idaho batholith and Challis intrusions have received far less attention than the other major Cordilleran batholiths, and most studies have focused on specific geographical areas or specific individual units. With the exception of King & Valley (2001), no workers have looked at the evolution of the system as a whole in a single study.

Previous work on the various suites of the Idaho batholith has shown that the intrusions in and adjacent to the Salmon River suture zone have a wide compositional range; however, the Atlanta and Bitterroot peraluminous suites have characteristic and overlapping compositions, such as a restricted SiO_2 range (70–74%), high Na_2O ($\geq$3·0%) and low K_2O/Na_2O (<1), high Sr ($\geq$500 ppm), and steeply sloping normalized rare earth element (REE) patterns (e.g. Hyndman, 1984; Criss & Fleck, 1987; Lewis *et al.*, 1987; Toth, 1987; Norman & Leeman, 1989; Clarke, 1990; Manduca *et al.*, 1992; Lee, 2004). Studies of the Challis intrusions (Motzer, 1985; Clarke, 1990; Lewis & Kiilsgaard, 1991; Norman *et al.*, 1992; Mitchell, 1997; Reppe, 1997; Robertson, 1997) have shown that the pink granite suite is characterized by high K_2O/Na_2O and Rb/Sr (both >1), enrichment in FeO, F, and some high field strength elements (HFSE) relative to large ion lithophile elements (LILE), and enriched but relatively flat REE patterns with large negative Eu anomalies. Comparatively few data exist for the early and late metaluminous suites.

Early batholith-wide studies of Sr and O isotopes recognized that the batholith interior has relatively radiogenic Sr and heavy oxygen and also delineated a series of large, low-$\delta^{18}O$ zones representing fossil hydrothermal systems surrounding some of the Challis intrusions (Armstrong *et al.*, 1977; Criss & Taylor, 1983; Criss & Fleck, 1987, 1990). With the exception of those by Clarke (1990) and King & Valley (2001), most other isotopic studies have focused on the suture zone (Fleck, 1990; Manduca *et al.*, 1992; Russell & Gabites, 2003; Fleck & Criss, 2007; King *et al.*, 2007), the northeastern corner of the Bitterroot lobe (Chase *et al.*, 1978; Shuster & Bickford, 1985; Mueller *et al.*, 1995), and individual Challis intrusions in southeastern Idaho (Mitchell, 1997; Reppe, 1997; Robertson, 1997). Several of these studies utilized Nd and Pb isotopes, but few of such data exist for vast stretches of the peraluminous batholith interior and the early and late metaluminous suites.

Differing views on the petrogenesis of portions of the batholith arose from these studies. In studies along the Salmon River suture zone, Fleck (1990) and Manduca *et al.* (1992) considered the border zone suite to be a product of three-component mixing between mantle-derived arc magmas, Precambrian metasedimentary rocks, and a poorly constrained third component. In contrast, Clarke (1990) considered these rocks, along with the early metaluminous suite, to be the product of variable degrees of partial melting of a heterogeneous tonalitic to gabbroic (meta-igneous) crustal source with little or no mantle input. Clarke (1990) considered the Atlanta peraluminous suite to have a similar origin, but with a lower degree of partial melting of an intermediate source at greater depth. The two-mica granites within the Atlanta peraluminous suite were modeled as a product of fractional crystallization of the biotite granodiorite magmas. Fleck (1990) also considered the origins of the Atlanta peraluminous suite, but his focus was on a marginal area near the suture zone where granites are intimately juxtaposed with Precambrian wall-rocks. Fleck (1990) considered the suite

in this area to be a mix of lower and upper crustal components.

Many of the early isotopic and U–Pb zircon studies on the Idaho batholith focused on the Bitterroot peraluminous suite, particularly the northeastern corner of the Bitterroot lobe. Various workers have been largely in agreement that the magmas here contained large fractions of Precambrian crustal material but have not agreed on whether they were pure crustal melts or the product of assimilation of old crust by primitive arc magmas (Chase *et al.*, 1978; Bickford *et al.*, 1981; Shuster & Bickford, 1984; Fleck & Criss, 1985; Toth & Stacey, 1992; Mueller *et al.*, 1995). Hyndman & Foster (1988) and Foster & Hyndman (1990) suggested that mafic rocks exposed in the central Bitterroot lobe represent mantle-derived arc magmas that provided the heat for crustal anatexis and then mingled and mixed with the crustal melts. Recent age information on these rocks (Gaschnig *et al.*, 2010) in conjunction with field relationships (Lewis *et al.*, 2007*a*), however, demonstrates that at least some of these mafic rocks are Eocene in age and were emplaced during the Challis magmatism.

Studies of the Challis intrusive province have generally suggested a lower (to middle) crustal source, based on a combination of trace element and Sr–Nd isotopic signatures (Fleck & Criss, 1985; Clarke, 1990; Lewis & Kiilsgaard, 1991; Larson & Geist, 1995; Mitchell, 1997; Reppe, 1997; Robertson, 1997). The contrasting characteristics of the quartz monzodiorite and pink granite suites have generally been attributed to melting at different crustal levels and/or, the incorporation of a minor mantle component into the quartz monzodiorite suite. In contrast, the early mafic to intermediate lavas of the Challis volcanic field have been modeled as melts of the lithospheric mantle (Norman & Mertzman, 1991; McKervey, 1998), owing to their primitive major and trace element chemistry, but comparatively evolved isotopic signature.

In one of the few studies to look at the major phases of both lobes of the batholith and the Challis intrusions, King & Valley (2001) came to a different conclusion from those of the previously mentioned workers. Based on oxygen isotopes in zircon and other minerals, they considered the whole system to be the result of juvenile arc magmas assimilating only limited amounts (≤15%) of Precambrian metasedimentary rocks.

METHODS

Major and trace elements

Rock samples were crushed using jaw-crushers. Aliquots of this material (20–25 g) were selected using a rotating splitter and ground to powders in agate ball mills. For X-ray fluorescence (XRF) analyses, 3·5 g aliquots of powder were mixed with 7 g of a lithium tetraborate flux and fused in graphite crucibles at ~1000°C. The resulting beads were then reground in tungsten-carbide shatterboxes and fused again under the same conditions. For inductively coupled plasma mass spectrometry (ICP-MS) analyses, 2 g powder aliquots were mixed with 2 g of lithium tetraborate flux and fused under the same conditions as for XRF aliquots. These were then reground in Fe shatterboxes and dissolved using a $HF–HNO_3–HClO_4$ acid mixture.

All XRF and ICP-MS analyses were conducted at Washington State University. XRF analyses followed the procedures of Johnson *et al.* (1999), and ICP-MS analyses followed the procedures of Knaack *et al.* (1994). Representative results are presented in Table 1 and the full results are presented in Supplementary Data Appendix B (available for downloading at http://¥www.¥petrology.¥oxfordjournals.¥org). Major and trace elements determined by XRF were normalized to 100% on an anhydrous basis.

Sr, Nd, Hf (whole-rock), and Pb isotopes

For Sr, Nd, and Hf whole-rock isotopic analyses, ~0·25 g aliquots of whole-rock powders were dissolved at high pressure in sealed, steel-jacketed Teflon bombs with a 10:1 mixture of concentrated HF and HNO_3 acids at 150°C for 5–7 days. After conversion from fluorides to chlorides, samples were spiked with mixed $^{149}Sm–^{150}Nd$ and $^{176}Lu–^{180}Hf$ tracers. Hf, Sr, Lu–Yb, and the light REE (LREE) were initially separated on cation exchange columns using AG 50W-X8 (200–400 mesh) resin. Hf aliquots were further purified using columns with Ln spec resin following the methods of Münker *et al.* (2001). Sr aliquots were purified using micro-columns (0·18 ml resin volume) with Sr-spec resin and HNO_3. Lu was separated from Yb on columns with Ln spec resin and HCl (Vervoort *et al.*, 2004). Nd and Sm were separated from the LREE aliquot on columns with HDEHP-coated Teflon powder and HCl (Vervoort & Blichert-Toft, 1999).

All analyses were conducted using a Thermo-Finnigan Neptune multicollector (MC)-ICP-MS system at Washington State University. Sr analyses were corrected for mass fractionation using $^{86}Sr/^{88}Sr = 0·1194$ and normalized using NBS-987. Nd analyses were corrected for mass fractionation using $^{146}Nd/^{144}Nd = 0·7219$ and normalized using the Ames Nd standard. Sm analyses were corrected for fractionation using $^{147}Sm/^{152}Sm = 0·56081$. Whole-rock Hf analyses were corrected for mass fractionation using $^{179}Hf/^{177}Hf = 0·7325$ and normalized using the JMC-475 standard. Lu measurements were made using the methods of Vervoort *et al.* (2004). All mass fractionation corrections were made using the exponential law.

The uncertainties on the Sr, Nd, and Hf isotopic compositions in Tables 2 and 3 reflect in-run error only, presented as two standard errors. The full uncertainties are better assessed from the reproducibility of the standards. The average reproducibilities (2 standard deviations) of

Table 1: Representative major and trace element analyses

	EMS					BZS	APS		
Sample:	07RMG12	07RMG37	07RMG40	07RMG41	08RMG20	07RMG50	07RMG25	07RMG29	07RMG46
SiO_2	66·0	66·6	62·8	55·7	65·5	64·1	72·8	74·5	72·7
TiO_2	0·473	0·677	0·878	1·10	0·792	0·706	0·140	0·102	0·171
Al_2O_3	16·8	15·3	16·1	17·1	16·6	16·4	15·4	14·5	15·4
FeO*	4·00	4·16	5·57	6·94	4·02	4·81	1·02	0·938	1·32
MnO	0·107	0·076	0·089	0·129	0·060	0·092	0·048	0·056	0·041
MgO	0·979	2·21	3·06	5·63	1·56	2·38	0·196	0·187	0·265
CaO	4·33	4·28	5·50	8·11	4·46	4·54	1·37	1·06	1·98
Na_2O	4·05	3·18	3·45	3·42	3·65	3·29	5·15	4·36	4·63
K_2O	2·76	3·08	2·07	1·22	2·72	3·08	3·62	4·04	3·13
P_2O_5	0·154	0·195	0·265	0·334	0·246	0·205	0·034	0·022	0·045
ASI	0·96	0·93	0·90	0·79	0·98	0·97	1·03	1·08	1·06
XRF									
Ni	n.d.	1	9	48	n.d.	n.d.	n.d.	n.d.	n.d.
Cr	6	33	48	223	6	13	3	4	3
Sc	8	11	14	22	7	11	1	3	3
V	57	91	123	170	69	96	3	6	9
Ba	1018	941	698	779	853	1870	1463	971	1551
Rb	117	104	70	30	101	79	80	125	73
Sr	832	526	672	939	672	627	527	292	659
Zr	323	173	201	131	270	178	109	68	117
Y	52	14	18	20	23	12	7	15	8
Nb	38	17	21	16	41	10	17	33	17
Ga	23	18	19	20	22	20	20	19	19
Cu	n.d.	n.d.	1	14	n.d.	n.d.	n.d.	n.d.	n.d.
Zn	58	63	72	95	74	90	42	40	52
Pb	11	12	8	9	9	8	17	35	15
La	63	39	47	43	83	56	20	11	25
Ce	121	77	89	80	156	94	41	21	39
Th	21	23	12	3	25	13	8	10	6
Nd	48	29	34	36	62	32	17	9	17
U	6	6	4	2	3	2	1	2	2
ICP-MS									
La	61·1	42·2	47·3	42·9		57·8	21·8	12·3	
Ce	119	74·1	89·8	82·2		99·6	40·32	23·04	
Pr	13·4	7·98	9·97	9·75		9·57	4·48	2·80	
Nd	48·5	27·8	35·1	36·9		30·9	15·91	10·59	
Sm	9·55	4·85	6·07	6·75		4·75	2·81	2·67	
Eu	1·94	1·27	1·59	2·08		1·24	0·936	0·608	
Gd	9·01	3·74	4·72	5·29		3·47	2·01	2·72	
Tb	1·49	0·519	0·654	0·774		0·456	0·246	0·451	
Dy	9·23	2·83	3·45	4·28		2·41	1·27	2·55	
Ho	1·95	0·530	0·678	0·825		0·442	0·236	0·495	
Er	5·31	1·33	1·68	2·07		1·13	0·591	1·32	
Tm	0·788	0·196	0·242	0·297		0·164	0·089	0·192	
Yb	4·97	1·20	1·51	1·76		0·982	0·530	1·27	
Lu	0·767	0·196	0·244	0·277		0·151	0·090	0·207	
Ba	998	935	694	764		1853	1472	971	
Th	20·3	24·4	12·5	4·87		15·8	5·81	7·77	
Nb	38·1	17·5	20·2	16·9		11·0	16·2	32·5	
Y	51·2	14·0	17·4	20·9		11·8	6·15	13·6	
Hf	8·47	4·72	5·00	3·43		4·65	2·78	2·25	
Ta	2·21	1·39	1·61	0·989		0·484	0·854	2·33	
U	4·33	4·74	2·57	1·20		1·40	1·05	2·49	
Pb	10·8	13·5	9·30	9·23		10·8	17·1	34·5	
Rb	114	102	67·6	29·0		76·7	79·2	121	
Cs	2·12	3·78	2·02	0·921		1·54	1·75	2·56	
Sr	818	548	655	1000		656	512	281	
Sc	7·33	10·5	13·7	20·6		11·2	1·23	1·83	
Zr	310	167	184	128		174	103	65·0	

(continued)

Table 1: Continued

	APS			LMS		BPS			
Sample:	07RMG52	07RMG54	08RMG11	01RL600	01RL729	06RMG02	06RMG03	06RMG07	07RMG66
SiO_2	74·5	75·2	74·7	61·9	63·6	72·1	72·6	71·9	71·2
TiO_2	0·111	0·123	0·126	0·776	0·554	0·247	0·230	0·202	0·195
Al_2O_3	14·6	14·1	14·7	17·1	17·3	15·7	15·2	15·6	16·2
FeO*	0·952	0·983	1·11	4·95	4·53	1·51	1·63	1·31	1·28
MnO	0·042	0·034	0·036	0·079	0·090	0·016	0·020	0·020	0·023
MgO	0·178	0·223	0·255	3·07	2·29	0·377	0·443	0·379	0·372
CaO	1·51	1·79	1·72	5·45	4·44	1·75	1·71	1·88	1·88
Na_2O	3·98	3·87	3·81	3·71	3·79	4·12	4·08	4·66	4·57
K_2O	3·84	3·34	3·35	2·47	2·98	3·76	3·79	3·56	3·82
P_2O_5	0·035	0·029	0·041	0·234	0·178	0·062	0·067	0·053	0·066
ASI	1·09	1·07	1·13	0·91	0·98	1·12	1·09	1·05	1·08
XRF									
Ni	n.d.	n.d.	n.d.	15	5	3	3	3	n.d.
Cr	2	7	4	46	16	3	3	3	0
Sc	0	2	3	11	9	4	4	3	2
V	1	3	6	99	76	14	18	12	13
Ba	1200	1531	898	921	1224	1651	1453	1536	1718
Rb	132	89	105	78	93	87	86	71	79
Sr	466	669	445	613	618	683	610	1054	1078
Zr	77	91	79	200	181	167	152	128	129
Y	9	11	9	15	15	8	16	8	10
Nb	14	12	15	10	8	5	6	4	5
Ga	21	19	18	21	20	18	17	18	19
Cu	n.d.	n.d.	n.d.	7	n.d.	1	4	n.d.	n.d.
Zn	56	44	36	80	66	33	37	34	35
Pb	18	17	17	9	12	17	22	22	25
La	34	24	19	39	59	40	69	30	34
Ce	63	51	35	77	110	76	129	56	59
Th	8	8	9	6	15	10	15	8	8
Nd	21	19	15	32	39	29	45	22	24
U	1	0	1	1	3				1
ICP-MS									
La	36·5	26·6	21·1		60·4	41·9	71·8	31·9	33·1
Ce	62·5	45·7	39·0		111	80·1	128	60·5	62·6
Pr	6·51	4·88	4·26		11·9	8·99	13·6	6·76	7·00
Nd	21·1	16·2	14·7		39·7	31·1	45·3	23·8	24·6
Sm	3·38	2·78	2·75		5·87	5·05	7·25	4·11	4·25
Eu	0·658	0·607	0·727		1·38	1·06	1·28	0·942	0·939
Gd	2·39	2·11	2·07		4·04	3·20	4·95	2·81	2·88
Tb	0·331	0·315	0·305		0·546	0·377	0·672	0·362	0·379
Dy	1·74	1·78	1·64		2·91	1·79	3·38	1·77	1·91
Ho	0·313	0·338	0·315		0·551	0·301	0·570	0·294	0·338
Er	0·755	0·911	0·842		1·47	0·712	1·29	0·678	0·890
Tm	0·105	0·134	0·122		0·217	0·100	0·165	0·098	0·124
Yb	0·622	0·854	0·795		1·39	0·612	0·972	0·582	0·765
Lu	0·091	0·132	0·123		0·234	0·103	0·147	0·102	0·120
Ba	1204	1542	912		1213	1683	1480	1561	1724
Th	7·28	6·74	6·62		14·8	11·5	15·9	7·55	8·32
Nb	14·7	12·6	14·3		8·86	5·24	6·72	4·65	5·14
Y	9·00	9·84	8·31		15·3	7·85	14·6	7·65	9·34
Hf	2·52	2·83	2·20		4·90	4·36	4·09	3·51	3·47
Ta	1·32	0·941	1·11		0·821	0·316	0·471	0·193	0·240
U	1·37	1·05	1·23		2·28	1·59	2·23	1·03	1·46
Pb	18·9	17·8	17·3		13·3	19·8	24·7	23·3	25·1
Rb	130·5	89·4	106·2		92·6	84·1	83·4	71·7	77·7
Cs	1·86	0·94	3·39		3·19	0·990	1·49	0·622	0·576
Sr	455	691	438		620	659	587	1062	1052
Sc	1·28	1·36	1·57		8·44	2·54	3·02	2·43	2·26
Zr	75·5	89·9	73·3		190	161	146	130	128

(continued)

Table 1: Continued

	BPS		BM			CI			
Sample:	07RMG70	08RMG28	06RMG06	08RMG08	08RMG30	06RMG05	07RMG10	07RMG23	07RMG24
SiO_2	72·7	72·2	59·7	53·1	60·5	66·1	69·0	65·7	75·8
TiO_2	0·144	0·179	0·916	1·94	0·672	0·322	0·504	0·600	0·200
Al_2O_3	15·5	15·7	15·9	16·4	15·2	17·1	15·0	16·6	13·3
FeO*	1·21	1·23	5·79	8·84	5·42	3·07	3·00	3·55	1·15
MnO	0·042	0·025	0·090	0·131	0·093	0·046	0·056	0·066	0·057
MgO	0·276	0·337	5·54	6·87	7·06	0·154	1·65	1·90	0·305
CaO	1·81	1·66	5·77	7·15	5·40	1·46	2·90	4·22	1·08
Na_2O	3·93	4·42	3·54	3·32	3·05	3·97	3·37	4·24	3·85
K_2O	3·92	3·77	2·27	1·41	2·19	7·48	4·08	2·57	4·03
P_2O_5	0·095	0·060	0·217	0·442	0·144	0·044	0·140	0·223	0·044
ASI	1·11	1·09	0·85	0·82	0·88	0·99	0·99	0·95	1·05
XRF									
Ni	n.d.	n.d.	73	149	148	3	1	8	n.d.
Cr	3	3	233	238	372	2	59	37	4
Sc	3	4	16	19	16	10	8	8	2
V	11	10	121	165	105	n.d.	47	55	13
Ba	1247	1478	764	896	581	733	943	1269	690
Rb	119	91	72	44	67	122	163	78	118
Sr	808	907	529	650	467	70	325	888	206
Zr	79	112	163	252	118	491	167	197	103
Y	11	13	12	21	13	15	19	14	16
Nb	9	6	9	22	5	10	10	14	24
Ga	19	20	18	20	18	20	19	21	16
Cu	n.d.	n.d.	17	45	24	5	4	n.d.	n.d.
Zn	37	39	67	99	64	41	51	73	43
Pb	23	23	10	4	11	20	14	13	24
La	16	33	27	37	16	311	22	41	26
Ce	34	65	54	79	29	497	45	77	48
Th	4	11	6	5	4	18	13	11	21
Nd	14	23	25	38	13	139	21	31	18
U	1	2		2		3	5	3	4
ICP-MS									
La	19·7	32·3	27·2	38·8	15·0	314·5	23·7	40·6	22·9
Ce	37·8	61·9	50·8	77·1	28·9	505	46·1	74·2	44·6
Pr	4·31	7·02	5·80	9·36	3·66	47·3	5·73	8·54	5·17
Nd	15·2	24·8	21·7	36·7	14·6	139	21·5	30·9	18·3
Sm	3·01	4·41	4·20	7·20	3·18	13·1	4·57	5·68	3·70
Eu	0·731	0·912	1·20	2·27	0·981	1·377	1·03	1·53	0·555
Gd	2·27	3·00	3·27	5·80	2·78	5·99	3·81	4·16	2·99
Tb	0·353	0·397	0·490	0·854	0·431	0·678	0·587	0·557	0·457
Dy	1·97	2·00	2·75	4·66	2·54	3·30	3·44	2·91	2·58
Ho	0·366	0·354	0·531	0·871	0·510	0·601	0·691	0·516	0·490
Er	0·958	0·891	1·34	2·13	1·35	1·57	1·84	1·30	1·33
Tm	0·137	0·128	0·190	0·286	0·192	0·220	0·274	0·180	0·211
Yb	0·832	0·770	1·15	1·71	1·22	1·32	1·73	1·09	1·40
Lu	0·132	0·121	0·181	0·254	0·192	0·216	0·276	0·170	0·226
Ba	1256	1461	749	876	577	750	944	1251	687
Th	4·23	8·25	6·72	4·95	5·16	18·7	15·5	10·8	18·8
Nb	9·49	5·91	9·56	22·2	4·66	9·49	10·4	14·5	23·0
Y	10·3	9·74	12·8	21·6	13·0	15·0	18·6	13·7	14·3
Hf	2·21	2·96	4·19	5·71	3·16	9·94	5·15	4·83	3·67
Ta	0·601	0·397	0·673	1·40	0·345	0·604	0·963	1·03	2·21
U	0·929	1·64	2·31	1·29	2·06	2·79	4·64	2·37	4·54
Pb	23·9	22·4	11·5	4·27	12·0	22·9	16·0	14·5	24·8
Rb	117	88·0	72·9	41·9	66·7	117	160	75·9	117
Cs	1·00	0·985	4·31	2·40	4·93	4·63	5·08	2·68	1·32
Sr	821	883	540	634	463	68·3	339	863	200
Sc	2·69	2·89	16·0	20·0	16·5	10·9	7·74	7·36	2·89
Zr	79·5	109	159	246	115	468	168	185	97·7

(continued)

Table 1: Continued

	CI		
Sample:	07RMG34	07RMG51	07RMG64
SiO_2	68·1	76·3	75·1
TiO_2	0·558	0·175	0·171
Al_2O_3	15·1	12·6	13·5
FeO*	3·38	1·35	1·64
MnO	0·057	0·040	0·034
MgO	1·47	0·179	0·148
CaO	2·85	0·58	0·70
Na_2O	3·75	3·92	4·27
K_2O	4·27	4·68	4·25
P_2O_5	0·157	0·028	0·035
ASI	0·94	1·00	1·05
XRF			
Ni	9	n.d.	n.d.
Cr	34	2	2
Sc	8	3	4
V	55	6	5
Ba	1445	248	242
Rb	128	173	191
Sr	455	49	74
Zr	266	193	186
Y	20	31	37
Nb	24	24	31
Ga	20	19	24
Cu	6	n.d.	n.d.
Zn	50	38	71
Pb	22	22	28
La	62	59	46
Ce	118	114	98
Th	25	21	30
Nd	42	43	40
U	5	6	11
ICP-MS			
La	63·7	61·2	44·9
Ce	116	118	94·5
Pr	12·4	13·1	11·3
Nd	41·8	44·9	40·8
Sm	6·66	7·81	8·72
Eu	1·42	0·385	0·350
Gd	4·94	6·32	7·06
Tb	0·667	0·974	1·16
Dy	3·65	5·64	6·74
Ho	0·700	1·12	1·31
Er	1·87	2·98	3·45
Tm	0·270	0·441	0·510
Yb	1·72	2·72	3·11
Lu	0·275	0·423	0·473
Ba	1456	251	237
Th	24·6	19·2	30·5
Nb	23·3	23·4	31·3
Y	18·3	29·3	34·5
Hf	6·70	6·33	7·27
Ta	1·73	1·68	2·58
U	4·71	5·21	10·5
Pb	23·0	23·7	27·7
Rb	123	169	188
Cs	2·73	4·40	5·04
Sr	439	48·5	72·0
Sc	7·01	2·54	2·54
Zr	246	186	185

Major element oxides are presented in weight per cent and trace elements are presented in parts per million. Major and trace elements determined by XRF have been normalized together to 100% anhydrous. ASI is aluminum saturation index, defined as Al/(Ca + Na + K). EMS, early metaluminous suite; BZS, border zone suite; APS, Atlanta peraluminous suite; LMS, late metaluminous suite; BPS, Bitterroot peraluminous suite; BM, Bitterroot mafic rocks; CI, Challis intrusions.

$^{87}Sr/^{86}Sr$, $^{143}Nd/^{144}Nd$, and $^{176}Hf/^{177}Hf$ on the NBS-987, Ames, and JMC-475 standards during the course of this study were ±0·00005, ±0·000020, and ±0·000014, respectively.

ε_{Nd} values were calculated using present-day values of $^{143}Nd/^{144}Nd = 0{\cdot}512630$ and $^{147}Sm/^{144}Nd = 0{\cdot}160$ for CHUR (Bouvier *et al.*, 2008). ε_{Hf} values were calculated using present-day values of $^{176}Hf/^{177}Hf = 0{\cdot}282785$ and $^{176}Lu/^{177}Hf = 0{\cdot}0336$ for CHUR (Bouvier *et al.*, 2008). Initial isotopic values were calculated using parent–daughter ratios determined by isotope dilution in the case of Nd and Hf isotopes and by Rb and Sr concentrations from XRF for Sr isotopes. Crystallization ages are based on the chronology given by Gaschnig *et al.* (2010). Sr results are given in Table 2 and Nd and Hf results are given in Table 3.

Pb isotopic compositions were determined on powder aliquots dissolved separately. These were washed and sonicated in 6M HCl at least once to remove any secondary Pb, rinsed with purified H_2O, and dissolved in sealed 15 ml Savillex™ beakers with a 10:1 HF–HNO_3 mixture on a hot plate at *c.* 120°C for 24 h. After conversion from fluorides to bromides, Pb was separated using BioRad AG

Table 2: Sr and Pb isotopic data

Sample no.	$^{87}Rb/^{86}Sr$*	$^{87}Sr/^{86}Sr$	$^{87}Sr/^{86}Sr$ (i)	Age (Ma)	$^{206}Pb/^{204}Pb$	$^{207}Pb/^{204}Pb$	$^{208}Pb/^{204}Pb$
Early metaluminous suite							
06RMG11					19·5305 ± 20	15·6717 ± 20	39·6451 ± 50
07RMG12	0·41	0·71460 ± 2	0·7140	95	20·6769 ± 43	15·7764 ± 33	41·2548 ± 81
07RMG35	0·35	0·70783 ± 2	0·7074	90	19·4047 ± 18	15·7056 ± 20	39·3458 ± 62
07RMG36				87	19·4382 ± 44	15·7055 ± 34	39·4268 ± 86
07RMG37					19·5114 ± 20	15·7095 ± 20	39·3168 ± 50
07RMG40	0·30	0·70681 ± 2	0·7064	92	19·4683 ± 41	15·7064 ± 40	39·2690 ± 93
07RMG40e	0·52	0·70716 ± 2	0·7065	92			
07RMG41	0·09	0·70652 ± 2	0·7064	99	19·5313 ± 42	15·7345 ± 33	39·2659 ± 82
07RMG58	0·42	0·70681 ± 3	0·7063	90	20·1273 ± 20	15·7687 ± 22	40·0670 ± 67
08RMG07	0·26	0·70901 ± 2	0·7087	94	19·4610 ± 18	15·6628 ± 21	39·2729 ± 63
08RMG20	0·43	0·70852 ± 2	0·7079	94	19·8914 ± 30	15·7522 ± 29	40·1020 ± 77
JV07-02					19·4002 ± 20	15·7078 ± 20	39·3978 ± 51
Border zone suite							
98IB34†	*0·13*	*0·70841*	*0·7082*	85	19·2667 ± 34	15·6845 ± 28	39·2372 ± 67
Atlanta peraluminous suite							
07RMG13	0·52	0·71616 ± 2	0·7156	78	21·4762 ± 27	15·8791 ± 27	41·5574 ± 56
07RMG25	0·44	0·71053 ± 3	0·7101	74	18·8753 ± 43	15·7385 ± 34	40·1588 ± 82
07RMG27	0·06	0·71017 ± 2	0·7101	72	18·0679 ± 42	15·5888 ± 34	39·3591 ± 82
07RMG28	0·22	0·71066 ± 2	0·7104	69	18·3224 ± 43	15·6443 ± 34	39·5570 ± 84
07RMG29	1·23	0·71624 ± 3	0·7150	68	17·8708 ± 45	15·6446 ± 36	40·1918 ± 89
07RMG43	0·26	0·70708 ± 3	0·7068	71	17·9727 ± 39	15·6099 ± 39	39·3849 ± 90
07RMG45	0·32	0·70956 ± 2	0·7092	77	19·0404 ± 18	15·7198 ± 21	39·6674 ± 64
07RMG52	0·82	0·70920 ± 2	0·7083	80	19·5813 ± 39	15·7397 ± 39	39·4030 ± 89
07RMG54	0·39	0·70878 ± 2	0·7083	80	19·2073 ± 20	15·7171 ± 22	39·3563 ± 64
07RMG55	0·26	0·70812 ± 2	0·7078	85	19·2537 ± 18	15·7165 ± 21	39·3149 ± 63
07RMG56	0·21	0·70803 ± 2	0·7078	76	19·0840 ± 18	15·7121 ± 20	39·3354 ± 62
08RMG11	0·69	0·71247 ± 2	0·7117	78	19·1356 ± 30	15·7289 ± 30	40·2889 ± 78
08RMG12	0·56	0·71010 ± 2	0·7095	78	19·2681 ± 30	15·6974 ± 29	39·2832 ± 77
08RMG13	0·35	0·71266 ± 3	0·7123	78	19·2200 ± 30	15·7378 ± 30	39·8548 ± 77
08RMG19	0·58	0·71368 ± 3	0·7130	78	19·0918 ± 30	15·7382 ± 30	40·1323 ± 78
10RMG041	1·17	0·71120 ± 16	0·7099	80	19·1428 ± 24	15·7448 ± 22	39·8539 ± 51
10RMG042	0·33	0·70795 ± 10	0·7076	82	19·2571 ± 24	15·6977 ± 22	39·2716 ± 51
10RMG043	2·29	0·71028 ± 19	0·7076	82	19·2610 ± 26	15·7019 ± 22	39·2364 ± 50
10RMG044					19·3039 ± 22	15·6994 ± 21	39·2208 ± 50
10NB356					19·1632 ± 27	15·7348 ± 26	40·2847 ± 56
10RL896					19·2812 ± 27	15·7174 ± 26	39·4274 ± 55
98IB68†	*0·55*	*0·71006*	*0·7094*	84	19·6166 ± 35	15·7560 ± 29	39·9407 ± 68
Late metaluminous suite							
01RL600	0·37	0·70879 ± 3	0·7084	73	19·3731 ± 20	15·6645 ± 20	39·1649 ± 50
01RL729	0·44	0·70881 ± 2	0·7084	71	18·9799 ± 18	15·6319 ± 20	38·8517 ± 62
06RMG01	0·24	0·70973 ± 2	0·7095	69	19·2343 ± 39	15·6650 ± 39	39·1982 ± 90
09RMG04	0·18	0·70794 ± 3	0·7078	72			
Bitterroot peraluminous suite							
06RMG02	0·37	0·71117 ± 2	0·7109	60	19·0581 ± 34	15·6607 ± 28	38·9369 ± 67
06RMG03	0·41	0·71158 ± 2	0·7112	66	19·0579 ± 39	15·6683 ± 39	38·9904 ± 90

(continued)

Table 2: Continued

Sample no.	$^{87}Rb/^{86}Sr$*	$^{87}Sr/^{86}Sr$	$^{87}Sr/^{86}Sr$ (i)	Age (Ma)	$^{206}Pb/^{204}Pb$	$^{207}Pb/^{204}Pb$	$^{208}Pb/^{204}Pb$
06RMG07	0·20	0·70919 ± 2	0·7090	60	18·2685 ± 20	15·5908 ± 20	38·1943 ± 50
06RMG08	0·24	0·70956 ± 3	0·7093	62	18·3935 ± 20	15·5985 ± 20	38·3809 ± 50
06RMG09					18·9698 ± 20	15·6500 ± 20	38·8224 ± 51
07RMG66	0·21	0·70918 ± 2	0·7090	60	18·3401 ± 18	15·5978 ± 21	38·2876 ± 63
07RMG70	0·43	0·71004 ± 2	0·7096	66	18·3416 ± 39	15·5906 ± 39	38·3483 ± 90
08RMG10	0·36	0·70965 ± 2	0·7093	60	18·3084 ± 30	15·5844 ± 30	38·2627 ± 78
08RMG26	0·27	0·70971 ± 2	0·7095	60			
08RMG28	0·29	0·70953 ± 2	0·7093	60			
98IB6†	*0·22*	*0·70934*	*0·7092*	59	18·3138 ± 20	15·5958 ± 20	38·2449 ± 51
98IB12†	*0·43*	*0·71574*	*0·7154*	56	19·4102 ± 19	15·7013 ± 21	39·2993 ± 64
98IB13†	*0·31*	*0·71085*	*0·7106*	54	18·0639 ± 39	15·5729 ± 39	38·2951 ± 89
Bitterroot mafic rocks							
07RMG03	0·16	0·70609 ± 2	0·7060	48	18·1890 ± 11	15·5541 ± 14	38·1215 ± 29
07RMG04	0·43	0·70605 ± 3	0·7058	47			
07RMG07	0·36	0·70687 ± 3	0·7066	57	18·9515 ± 11	15·6204 ± 14	38·7262 ± 26
08RMG08	0·19	0·70555 ± 2	0·7054	57	18·1730 ± 18	15·5483 ± 21	38·1608 ± 65
08RMG30	0·41	0·70598 ± 2	0·7056	57	18·9074 ± 23	15·6204 ± 23	38·6779 ± 53
08RMG31	0·35	0·70710 ± 2	0·7068	57	18·9902 ± 25	15·6252 ± 23	38·7563 ± 57
09RMG02	0·48	0·70585 ± 3	0·7055	57			
Challis intrusive rocks‡							
06RMG05					18·8363 ± 43	15·6224 ± 34	38·7762 ± 82
07RMG10	1·45	0·70926 ± 2	0·7082	51	19·3781 ± 34	15·6715 ± 28	39·1420 ± 68
07RMG23	0·25	0·70668 ± 2	0·7065	47	18·8804 ± 34	15·6494 ± 28	39·1332 ± 67
07RMG33					17·7789 ± 18	15·5875 ± 22	39·1664 ± 66
07RMG34	0·81	0·70998 ± 2	0·7094	48	17·8837 ± 43	15·5692 ± 34	38·9694 ± 83
07RMG51	10·2	0·71428 ± 2	0·7073	48	17·9635 ± 42	15·5260 ± 34	37·9581 ± 81
07RMG64	7·49	0·71270 ± 2	0·7076	48	18·5087 ± 42	15·5817 ± 33	38·4149 ± 80
07RMG65	2·25	0·70854 ± 3	0·7070	48	18·5846 ± 42	15·5911 ± 33	38·4848 ± 80
08AMT019	0·16	0·70556 ± 2	0·7055	48	17·0387 ± 18	15·3790 ± 20	36·8737 ± 62
08RAB026	11·9	0·71305 ± 2	0·7051	47	18·4977 ± 18	15·5793 ± 21	38·3139 ± 63
08RMG32					17·8464 ± 18	15·5397 ± 21	39·0497 ± 65
10RL894	0·72	0·70692 ± 2	0·7064	48	19·1366 ± 22	15·6652 ± 21	39·0809 ± 49
10RL897	1·2	0·70942 ± 1	0·7086	48			
98IB24†	*1·58*	*0·70790*	*0·7069*	46	18·0421 ± 42	15·5336 ± 33	38·0855 ± 80
98IB61	3·47	0·71040 ± 2	0·7083	43	18·0577 ± 42	15·5676 ± 33	39·1076 ± 80

*$^{87}Rb/^{86}Sr$ are calculated from Rb and Sr concentrations obtained by XRF and presented in Supplementary Data Appendix B.
†Sr data for samples in italics were determined by King *et al*. (2007) and are shown here alongside new Pb data for completeness.
‡Calculated initial ratios for Challis and Atlanta peraluminous samples with $^{87}Rb/^{86}Sr > 1$ are less precise owing to the greater effect of uncertainy in Rb and Sr concentrations and age.
Uncertainties on Sr measurements are internal only and represent two standard errors. Uncertainties on Pb include reproducibility of the standard.

1-X8 anion resin. Pb isotopic compositions were measured on the same MC-ICP-MS instrument as Sr, Nd, and Hf, using the thallium doping procedure described by White *et al*. (2000). Unknowns were doped with 30 ppb Tl and run alternately with the NBS-981 standard with a concentration of 150 ppb Pb and 30 ppb Tl. After correcting for the mass bias using the thallium, samples were normalized to the triple-spike values for NBS-981 from Galer &

Table 3: Sm–Nd and Lu–Hf isotopic data

Sample no.	Sm	Nd	$^{147}Sm/^{144}Nd$	$^{143}Nd/^{144}Nd$	$^{143}Nd/^{144}Nd$ (initial)	ε_{Nd}	ε_{Nd} (initial)	Lu	Hf	$^{176}Lu/^{177}Hf$	$^{176}Hf/^{177}Hf$	$^{176}Hf/^{177}Hf(i)$	ε_{Hf}	ε_{Hf} (initial)	Age (Ma)
Early metaluminous suite															
07RMG12	9·02	47·9	0·1139	0·512232 ± 9	0·512161	−7·8	−6·8 ± 0·2	0·710	8·67	0·0116	0·282280 ± 9	0·282260	−17·8	−16·5 ± 0·3	95
07RMG35	6·32	39·4	0·0969	0·512218 ± 9	0·512161	−8·0	−6·9 ± 0·2	0·138	5·63	0·0035	0·282403 ± 10	0·282397	−13·5	−11·7 ± 0·3	90
07RMG36	5·96	35·8	0·1007	0·512243 ± 6	0·512186	−7·5	−6·5 ± 0·1	0·162	5·67	0·0041	0·282371 ± 6	0·282364	−14·6	−12·9 ± 0·2	87
07RMG40	5·50	33·3	0·1000	0·512315 ± 9	0·512255	−6·1	−5·0 ± 0·2	0·228	5·06	0·0064	0·282446 ± 11	0·282435	−12·0	−10·3 ± 0·4	92
07RMG40e	8·93	53·5	0·1011	0·512326 ± 8	0·512265	−5·9	−4·8 ± 0·2	0·421	7·16	0·0083	0·282496 ± 11	0·282482	−10·2	−8·7 ± 0·4	92
07RMG41	6·19	35·6	0·1051	0·512301 ± 5	0·512233	−6·4	−5·3 ± 0·1	0·261	3·15	0·0118	0·282435 ± 7	0·282413	−12·4	−11·0 ± 0·2	99
07RMG58	7·88	51·5	0·0925	0·512297 ± 5	0·512242	−6·5	−5·3 ± 0·1	0·233	6·54	0·0051	0·282425 ± 6	0·282417	−12·7	−11·0 ± 0·2	90
08RMG07	3·89	19·5	0·1206	0·512242 ± 8	0·512167	−7·6	−6·7 ± 0·2								94
08RMG20	9·29	56·9	0·0987	0·512229 ± 10	0·512168	−7·8	−6·7 ± 0·2								94
Border zone suite															
98IB34	3·84	27·9	0·0831	0·512204 ± 8	0·512158	−8·3	−7·1 ± 0·2								85
Atlanta peraluminous suite															
07RMG13	3·24	16·1	0·1216	0·512059 ± 10	0·511997	−11·1	−10·4 ± 0·2								78
07RMG25	2·63	15·7	0·1015	0·511927 ± 9	0·511878	−13·7	−12·8 ± 0·2	0·086	2·88	0·0042	0·282234 ± 12	0·282228	−19·5	−18·1 ± 0·4	74
07RMG27	2·43	17·6	0·0832	0·511849 ± 9	0·511810	−15·2	−14·2 ± 0·2	0·048	2·61	0·0026	0·282244 ± 9	0·282240	−19·1	−17·7 ± 0·3	72
07RMG28	1·90	13·0	0·0878	0·511789 ± 10	0·511749	−16·4	−15·5 ± 0·2	0·035	2·09	0·0024	0·282163 ± 8	0·282160	−22·0	−20·6 ± 0·3	69
07RMG29	2·47	10·0	0·1490	0·511654 ± 10	0·511587	−19·0	−18·6 ± 0·2	0·187	2·18	0·0122	0·282020 ± 10	0·282004	−27·1	−26·1 ± 0·3	68
07RMG43	1·72	9·49	0·1097	0·511909 ± 7	0·511858	−14·1	−13·3 ± 0·1	0·109	2·11	0·0073	0·282104 ± 7	0·282094	−24·1	−22·8 ± 0·3	71
07RMG52	2·86	18·6	0·0927	0·512184 ± 6	0·512136	−8·7	−7·6 ± 0·1	0·083	2·50	0·0047	0·282329 ± 6	0·282322	−16·1	−14·6 ± 0·2	80
07RMG54	2·48	15·3	0·0981	0·512096 ± 6	0·512045	−10·4	−9·4 ± 0·1	0·129	2·77	0·0066	0·282354 ± 6	0·282344	−15·2	−13·8 ± 0·2	80
07RMG55	2·43	14·2	0·1032	0·512145 ± 11	0·512088	−9·5	−8·4 ± 0·2								85
07RMG56	3·83	26·2	0·0886	0·512095 ± 10	0·512051	−10·4	−9·4 ± 0·2	0·138	4·48	0·0044	0·282375 ± 7	0·282369	−14·5	−13·0 ± 0·3	76
08RMG11	2·31	13·0	0·1073	0·511859 ± 9	0·511804	−15·0	−14·2 ± 0·2								78
08RMG12	1·89	11·4	0·1003	0·512078 ± 8	0·512027	−10·8	−9·8 ± 0·2								78
08RMG13	3·19	19·9	0·0970	0·511885 ± 7	0·511836	−14·5	−13·5 ± 0·1								78
08RMG19	2·86	16·4	0·1053	0·511846 ± 10	0·511792	−15·3	−14·4 ± 0·2								78
10RMG041	1·62	5·32	0·1846	0·511957 ± 13	0·511858	−13·1	−13·0 ± 0·3	0·216	1·15	0·0266	0·282298 ± 4	0·282257	−17·2	−16·9 ± 0·2	82
10RMG042	3·29	21·8	0·0911	0·512186 ± 10	0·512137	−8·7	−7·6 ± 0·2	0·108	3·09	0·0049	0·282462 ± 3	0·282454	−11·4	−9·9 ± 0·1	82
10RMG043	2·63	8·8	0·1814	0·512220 ± 9	0·512125	−8·0	−7·9 ± 0·2								80
98IB53	2·59	13·0	0·1205	0·512097 ± 9	0·512039	−10·4	−9·7 ± 0·2								74
98IB68	5·30	32·4	0·0989	0·512102 ± 8	0·512047	−10·3	−9·3 ± 0·2								84
Late metaluminous suite															
01RL600	5·05	32·1	0·0952	0·512049 ± 10	0·512003	−11·3	−10·4 ± 0·2								73
01RL729	5·27	37·2	0·0855	0·511877 ± 6	0·511838	−14·7	−13·7 ± 0·1	0·222	4·68	0·0067	0·282280 ± 8	0·282271	−17·9	−16·6 ± 0·3	71

(continued)

Table 3: Continued

Sample no.	Sm	Nd	$^{147}Sm/^{144}Nd$	$^{143}Nd/^{144}Nd$	$^{143}Nd/^{144}Nd$ (initial)	ε_{Nd}	ε_{Nd} (initial)	Lu	Hf	$^{176}Lu/^{177}Hf$	$^{176}Hf/^{177}Hf$	$^{176}Hf/^{177}Hf$(i)	ε_{Hf}	ε_{Hf} (initial)	Age (Ma)
06RMG01	4·91	28·9	0·1028	0·511989 ± 10	0·511943	−12·5	−11·7 ± 0·2								69
09RMG04	4·79	25·8	0·1122	0·512092 ± 12	0·512040	−10·5	−9·7 ± 0·2								71
Bitterroot peraluminous suite															
06RMG02	4·55	29·2	0·0942	0·511806 ± 17	0·511769	−16·1	−15·3 ± 0·3								60
06RMG03	6·59	43·2	0·0923	0·511870 ± 8	0·511830	−14·8	−13·9 ± 0·2	0·138	4·23	0·0046	0·282190 ± 10	0·282184	−21·0	−19·8 ± 0·3	66
06RMG07	3·47	21·2	0·0989	0·511786 ± 7	0·511748	−16·5	−15·7 ± 0·1	0·090	3·60	0·0036	0·282133 ± 8	0·282129	−23·1	−21·9 ± 0·3	60
06RMG08	4·86	28·7	0·1023	0·511779 ± 8	0·511737	−16·6	−15·9 ± 0·2	0·101	4·40	0·0033	0·282185 ± 8	0·282181	−21·2	−20·0 ± 0·3	62
06RMG09	2·35	12·1	0·1177	0·511858 ± 9	0·511818	−15·1	−14·5 ± 0·2	0·189	2·74	0·0098	0·282279 ± 9	0·282269	−17·9	−17·1 ± 0·3	52
07RMG66	3·80	22·9	0·1003	0·511755 ± 6	0·511716	−17·1	−16·3 ± 0·1	0·140	3·56	0·0056	0·282004 ± 5	0·281998	−27·6	−26·5 ± 0·2	60
07RMG70	2·71	15·0	0·1093	0·511767 ± 6	0·511719	−16·8	−16·1 ± 0·1	0·130	2·24	0·0082	0·282166 ± 7	0·282156	−21·9	−20·8 ± 0·3	66
08RMG10	2·51	14·2	0·1071	0·511782 ± 9	0·511740	−16·5	−15·9 ± 0·2								60
08RMG26	3·69	21·8	0·1023	0·511765 ± 9	0·511725	−16·9	−16·2 ± 0·2								60
08RMG28	4·53	25·8	0·1062	0·511786 ± 9	0·511744	−16·5	−15·8 ± 0·2								60
98IB12	2·03	11·3	0·1082	0·511831 ± 8	0·511792	−15·6	−15·0 ± 0·1								56
98IB13	1·66	9·85	0·1020	0·511763 ± 21	0·511727	−16·9	−16·3 ± 0·4								54
98IB6	3·51	23·5	0·0903	0·511755 ± 7	0·511720	−17·1	−16·3 ± 0·1								59
Bitterroot mafic rocks															
07RMG03	3·75	17·0	0·1330	0·512124 ± 11	0·512082	−9·9	−9·5 ± 0·2								48
07RMG04	3·59	18·9	0·1150	0·512392 ± 7	0·512357	−4·6	−4·2 ± 0·1	0·195	4·14	0·0067	0·282609 ± 7	0·282603	−6·2	−5·4 ± 0·3	47
07RMG07	3·34	15·5	0·1303	0·512309 ± 8	0·512260	−6·3	−5·8 ± 0·2								57
08RMG08	8·09	43·8	0·1116	0·512465 ± 1	0·512423	−3·2	−2·6 ± 0·0								57
08RMG31	3·34	14·7	0·1373	0·512343 ± 8	0·512292	−5·6	−5·2 ± 0·2								57
08RMG30	2·81	13·6	0·1253	0·512634 ± 9	0·512587	0·1	0·6 ± 0·2								57
09RMG02	3·73	18·8	0·1197	0·512528 ± 9	0·512484	−2·0	−1·4 ± 0·2								57
Challis intrusive rocks															
06RMG05	11·7	129	0·0548	0·512422 ± 6	0·512404	−4·1	−3·2 ± 0·1	0·208	10·3	0·0029	0·282659 ± 7	0·282656	−4·5	−3·5 ± 0·2	49
07RMG10	4·19	20·7	0·1224	0·512398 ± 7	0·512357	−4·5	−4·0 ± 0·1	0·258	4·71	0·0078	0·282599 ± 7	0·282592	−6·6	−5·7 ± 0·2	51
07RMG23	5·28	30·4	0·1049	0·512337 ± 9	0·512305	−5·7	−5·2 ± 0·2	0·158	4·87	0·0046	0·282322 ± 11	0·282318	−16·4	−15·5 ± 0·4	47
07RMG34	6·21	40·3	0·0933	0·511767 ± 11	0·511737	−16·8	−16·2 ± 0·2	0·264	7·28	0·0051	0·282010 ± 10	0·282005	−27·4	−26·5 ± 0·4	48
07RMG51	7·10	41·4	0·1036	0·512088 ± 10	0·512055	−10·6	−10·0 ± 0·2	0·395	6·19	0·0091	0·282428 ± 10	0·282420	−12·6	−11·9 ± 0·4	48
07RMG64	8·01	38·9	0·1247	0·512312 ± 5	0·512273	−6·2	−5·8 ± 0·1	0·466	7·28	0·0091	0·282585 ± 7	0·282577	−7·1	−6·3 ± 0·2	48
07RMG65	5·33	31·4	0·1029	0·512327 ± 7	0·512295	−5·9	−5·3 ± 0·1	0·217	5·34	0·0058	0·282576 ± 7	0·282571	−7·4	−6·5 ± 0·2	48
08AMT019	1·94	9·33	0·1255	0·511782 ± 8	0·511743	−16·5	−16·1 ± 0·2	0·136	2·28	0·0085	0·282206 ± 7	0·282198	−20·5	−19·7 ± 0·2	48
08RAB026	5·10	21·0	0·1469	0·512268 ± 10	0·512223	−7·1	−6·8 ± 0·2								46
08RMG32	0·907	7·45	0·0736	0·512055 ± 7	0·512033	−11·2	−10·5 ± 0·1	0·408	6·29	0·0092	0·282264 ± 7	0·282256	−18·4	−17·7 ± 0·2	45
10RL894	7·51	43·1	0·1053	0·512407 ± 9	0·512374	−4·3	−3·8 ± 0·2								48
10RL897	10·6	66·9	0·0960	0·511825 ± 12	0·511795	−15·7	−15·1 ± 0·2								48
98IB22	4·49	27·8	0·0975	0·511946 ± 8	0·511915	−13·4	−12·8 ± 0·2								48
98IB24	4·74	33·8	0·0848	0·511964 ± 8	0·511938	−13·0	−12·3 ± 0·2								46
98IB61	5·47	27·8	0·1188	0·511800 ± 9	0·511766	−16·2	−15·8 ± 0·2								43

Quoted uncertainties are internal only and represent 2 standard errors.

Abouchami (1998). Pb isotopic ratios are presented here as measured present-day values. For most samples, radiogenic in-growth owing to *in situ* decay of U and Th is relatively trivial in the last 40–100 Myr compared with the wide variation seen in the samples. However, several samples of the early metaluminous suite are exceptional in this regard because of their high U/Pb and Th/Pb ratios, as determined by ICP-MS trace element analysis. For these samples, radiogenic in-growth accounts for the bulk of the within-suite variation. Pb results are presented in Table 2.

Zircon Hf isotopic analysis

All zircons analyzed for Hf isotopes here were previously age-characterized. Samples with names containing RMG, RL, and 98IB were dated by LA-ICP-MS and their ages were reported by Gaschnig *et al.* (2010). Samples 01KL104, 01KL107, 01KL111, MC13-91, and MC15-91 were dated by K. Lund and J. Aleinikoff using isotope dilution thermal ionization mass spectrometry (ID-TIMS) and sensitive high-resolution ion microprobe (SHRIMP) (Lund *et al.*, 2008; K. Lund, personal communication, 2008; Unruh *et al.*, 2008), and samples 01-53, 01-54, 99-1, 99-2, 99MG, GP-1, and GP-3 were dated by W. McClelland using SHRIMP (McClelland & Oldow, 2007; Murphy, 2007; Giorgis *et al.*, 2008).

In situ laser ablation (LA)-MC-ICP-MS Hf isotope analyses were conducted at Washington State University using a New Wave 213 nm UP Nd:YAG laser coupled to a Thermo-Finnigan Neptune MC-ICP-MS system with nine Faraday collectors. The laser was operated at a pulse rate of 10 Hz and power density of 10–12 J cm^{-2} with a spot size of 40 μm, except in a few cases where smaller grains and narrower zones required a smaller spot size of 30 μm. The carrier gas consisted of purified He with small quantities of N_2 to minimize oxide formation and increase sensitivity. Analyses consisted of 60, 1 s measurements in static mode.

The largest obstacle in LA-MC-ICP-MS Hf isotopic analysis is the isobaric interference of ^{176}Yb and ^{176}Lu on ^{176}Hf (e.g. Woodhead *et al.*, 2004). Whereas the extremely low ^{176}Lu/^{177}Hf in zircon minimizes the effect of the ^{176}Lu interference, ^{176}Yb can form >10% of the total signal at mass 176 and provides the largest source of uncertainty in the measurement. To correct for the Yb interference, a partially empirical approach was used, where a modified Yb isotopic composition was used to calculate the measured Yb interference, and the Yb mass bias was determined by the relationship $\beta_{Yb} = x \times \beta_{Hf}$. The value for x was determined by analyzing the zircon standards 91500, FC1, and R33 and adjusting the x value to best fit the known ^{176}Hf/^{177}Hf values determined on chemically purified solutions. The x value and modified ^{176}Yb/^{173}Yb were then used to calculate the Hf isotopic composition of the unknowns.

Because of the difficulty in correcting for the Yb interference and other sources of error such as instrumental bias and matrix effects, the internal measurement error by itself is often considerably less than the total uncertainty; the latter is difficult to assess. Based on the deviation of ^{176}Hf/^{177}Hf values determined by the *in situ* method on the standards from the values determined by solution analysis, we estimate the total uncertainty to be *c.* ±2 ε units.

To double-check the accuracy of the LA-MC-ICP-MS, we also conducted solution ID-MC-ICP-MS analysis on single zircons from a few samples with simple U–Pb and Hf systematics (i.e. those zircons with no inheritence), following the methods of Goodge & Vervoort (2006). Single zircons were dissolved in 0·5 ml Savillex™ vials at 250°C with HF–HNO_3 (~10:1) for 48 h. After dissolution and conversion to chlorides, solutions were spiked with a mixed ^{176}Lu–^{180}Hf tracer (Vervoort *et al.*, 2004). Hf and Lu were separated using micro-columns with Dowex AG50W-X12 cation resin and analyzed at Washington State University by MC-ICP-MS. Hf analyses were normalized to the JMC-475 standard, and Lu analyses followed the procedures of Vervoort *et al.* (2004). All zircon Hf isotopic data are presented in Supplementary Data Appendix C.

RESULTS

Major and trace element geochemistry

Major and trace element data are reported in Table 1 and Supplementary Data Appendix B. We focus only on the key characteristics here because detailed description and modeling of the major and trace element compositions of portions of the Idaho batholith and Challis intrusive province have been previously undertaken by many of the workers cited above. The major element compositions of the Idaho batholith and Challis intrusive province are shown and compared with other Cordilleran batholiths using the modified alkali–lime index (MALI; $Na_2O + K_2O - CaO$) and Fe* [$FeO_T/(MgO + FeO_T)$] discriminants of Frost *et al.* (2001) (Fig. 2). The early metaluminous, border zone, and late metaluminous suites generally straddle the calcic and calc-alkalic fields, are magnesian, and largely overlap fields for the western (Truschel, 1996) and eastern (Gray *et al.*, 2008) Cretaceous Sierra Nevada batholith. The Atlanta and Bitterroot peraluminous suites occupy a limited range of high SiO_2 values and are primarily calcic to calc-alkalic and magnesian. The Atlanta peraluminous suite tends to have a lower average MALI value than the Bitterroot, and both suites contain outliers with higher MALI and Fe*. The peraluminous suites are consistently more silicic than Sierran granitoids, with the exception of Sierran aplites and leucocratic granite porphyries (Gray *et al.*, 2008). The Bitterroot mafic rocks fall on the same MALI trend as the metaluminous and border zone suites, but are consistently

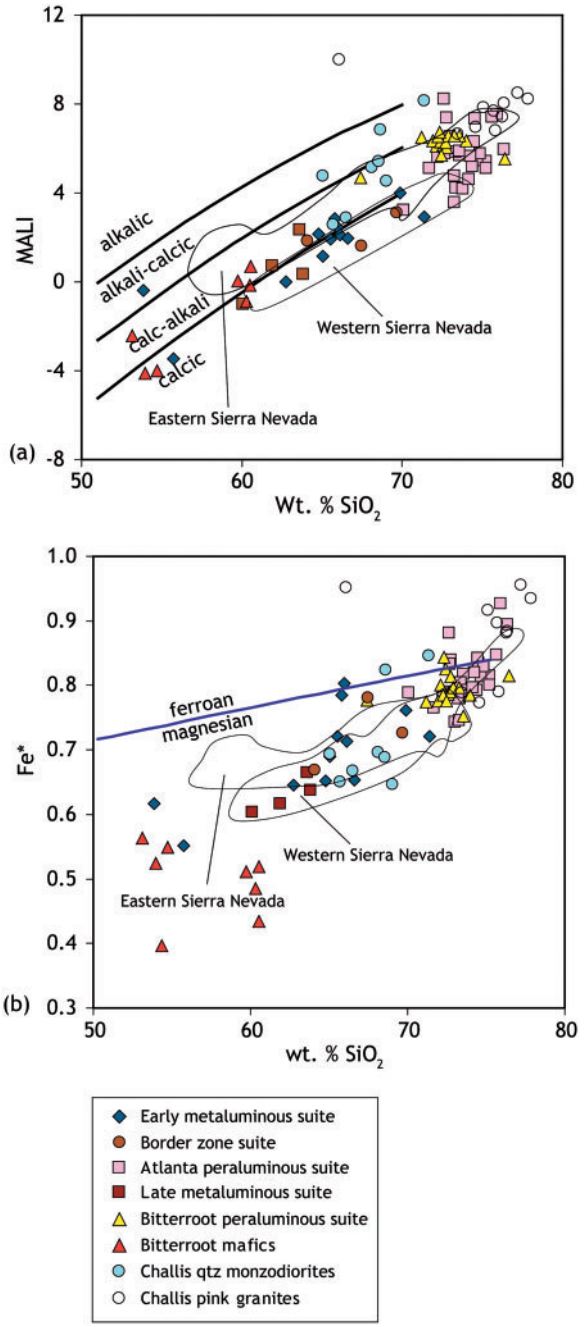

Fig. 2. Major element characteristics of Idaho batholith and Challis samples and classification using (a) the modified alkali–lime index (MALI; $K_2O + Na_2O - CaO$) and (b) Fe* [$FeO_T/(MgO + FeO_T)$] of Frost *et al.* (2001). Fields for western (Truschel, 1996) and eastern (Gray *et al.*, 2008) Sierra Nevada batholith rocks are shown for comparison.

less ferroan than other Idaho batholith, Challis, or Sierran rocks. Challis rocks differ from the suites of the Idaho batholith primarily by extending to both higher MALI and Fe* values and higher SiO_2 values.

Figure 3 displays some major element characteristics of the Idaho batholith and Challis rocks as a function of age. It is clear from this and Fig. 2 that the Atlanta and Bitterroot peraluminous suites have a narrow range of major element compositions compared with the other suites and are similar to each other. Although they share some trace element characteristics, subtle but important differences exist. The Atlanta peraluminous suite is characterized by lower LILE/HFSE and LREE/HFSE ratios (Fig. 4) and comparatively lower average Sr and higher Eu/Eu* (Fig. 5a). These differences are important because high LILE/HFSE and LREE/HFSE ratios, particularly depletion of Ta and Nb relative to LILE and LREE, are a persistent feature in arc magmatism (e.g. Pearce, 1982), and provide important information about the source of the Atlanta peraluminous suite. As previously mentioned, Challis rocks are commonly potassic ($K_2O/Na_2O > 1$) in contrast to the sodic rocks of all the Idaho batholith suites (Fig. 3c), and the pink granite suite in particular shows high Rb/Sr, and HFSE enrichment relative to LILE and LREE. The Challis quartz monzodiorite suite, however, has geochemical characteristics that are similar to those of the border zone, early metaluminous, and late metaluminous suites.

Another key trace element characteristic of the Idaho batholith–Challis system is the broadly higher La/Yb and Sr/Y and lower Yb and Y (Fig. 5b and c) of the Atlanta and Bitterroot peraluminous suites compared with the other suites, particularly the early metaluminous suite and Challis pink granites, which are the oldest and youngest units in the system, respectively.

Whole-rock Sr, Nd, and Hf (whole-rock) isotopes

Most of the components of the Idaho batholith have significant overlap in their Sr isotopic compositions based on our new data (Fig. 6a and b) and data from the literature (Armstrong *et al.*, 1977; Chase *et al.*, 1978; Fleck & Criss, 1985, 2007; Shuster & Bickford, 1985; Criss & Fleck, 1987; Clarke, 1990; Manduca *et al.*, 1992; Mitchell, 1997; Reppe, 1997; Robertson, 1997; King *et al.*, 2007; Unruh *et al.*, 2008). Essentially all suites (except for the Bitterroot mafic rocks) have initial $^{87}Sr/^{86}Sr$ values varying from 0·706 to 0·709 but with outliers up to 0·716; the higher values are more common in the two peraluminous suites. The Bitterroot mafic rocks have a narrow range in composition ($^{87}Sr/^{86}Sr_i = 0{\cdot}705–0{\cdot}707$). The Challis intrusions have a larger isotopic range ($^{87}Sr/^{86}Sr_i = 0{\cdot}705–0{\cdot}715$), with the plutons from northern Idaho having lower values.

In contrast to Sr, the suites of the Idaho batholith each have distinct and characteristic ranges of Nd isotopic compositions, and the system as a whole shows a striking decrease in $\varepsilon_{Nd(i)}$ values with time prior to ~50 Ma (Fig. 7a). This trend is even more pronounced if the juvenile mid-Cretaceous plutons of the Salmon River suture zone

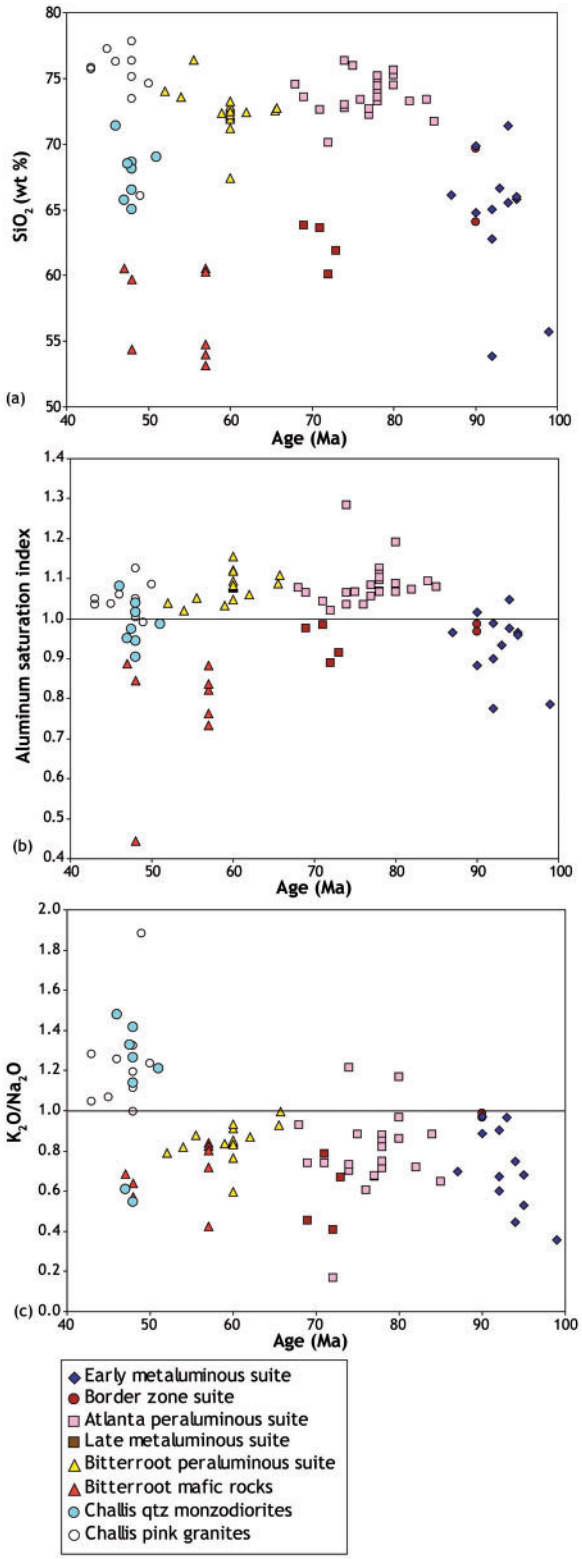

Fig. 3. Variation of (a) SiO_2, (b) aluminium saturation index and (c) K_2O/Na_2O vs age for the Idaho batholith and Challis samples.

and Blue Mountains Province are also considered (Fleck, 1990; Fleck & Criss, 2007; Unruh *et al.*, 2008), which have consistently positive epsilon values. The early metaluminous suite occupies a narrow range of −5 to −7 and the coeval border zone suite (Clarke, 1990; Fleck, 1990; Fleck & Criss, 2007; Unruh *et al.*, 2008) has broadly similar epsilon values but with a slightly greater range (Fig. 6). Our data for the Atlanta peraluminous suite have a larger range in epsilon values, with an average of about −9 and with distinctly lower values in certain geographical areas, such as south of the latitude of Stanley (~44°N). Our samples from the previously uncharacterized late metaluminous suite have $\varepsilon_{Nd(i)}$ values between −10 and −14. The Bitterroot peraluminous suite yielded consistent values between −14 and −16. Samples of mafic rocks within the Bitterroot lobe range from *c.* +1 to −6, with the exception of a pyroxenite cumulate mass of uncertain age (sample 07RMG03), which gave a value of −10. The 50–43 Ma Challis intrusions display the full Nd isotopic variation seen in the Idaho batholith, with $\varepsilon_{Nd(i)}$ values from −4 to −21. The more radiogenic values are generally more common in northern Idaho (i.e. north of 45°N) than southern Idaho.

Hf whole-rock isotopic data have similar ranges, patterns, and trends to Nd (Fig. 7b), with a shift to less radiogenic values prior to 50 Ma, although some are displaced to lower ε_{Hf} value for a given ε_{Nd} value.

Pb isotopes

Many suites of the Idaho batholith and Challis magmatism define distinct fields and arrays in $^{207}Pb/^{204}Pb$ vs $^{206}Pb/^{204}Pb$ space (Fig. 8). The early metaluminous and Atlanta peraluminous suites have distinctly higher $^{206}Pb/^{204}Pb$ and $^{207}Pb/^{204}Pb$ values, respectively, than the other suites. The high $^{206}Pb/^{204}Pb$ of the early metaluminous suite is due in part to *in situ* radiogenic decay but these samples still plot as a distinct field even when corrected for in-growth. The less radiogenic outliers (with $^{206}Pb/^{204}Pb < 18{\cdot}5$) from the Atlanta peraluminous suite are geographically distinct in that they are from the southernmost samples. In contrast to the early metaluminous and Atlanta peraluminous suites, the Bitterroot peraluminous suite forms a linear array with overall less radiogenic compositions in $^{207}Pb/^{204}Pb$ vs $^{206}Pb/^{204}Pb$ space. The Challis plutons form distinct fields based on location and are shown accordingly. Northern Challis plutons (defined as those north of 45°N) form a linear array parallel to the Bitterroot peraluminous suite, whereas southern Challis plutons are distinct and the least radiogenic overall. The late metaluminous and Bitterroot mafic rocks plot between the northern Challis and early metaluminous rocks.

The various suites have generally similar patterns in $^{208}Pb/^{204}Pb$ vs $^{206}Pb/^{204}Pb$ space (Fig. 8b). Two exceptions are the relatively collinear nature of the Bitterroot peraluminous suite, Bitterroot mafic rocks and northern Challis

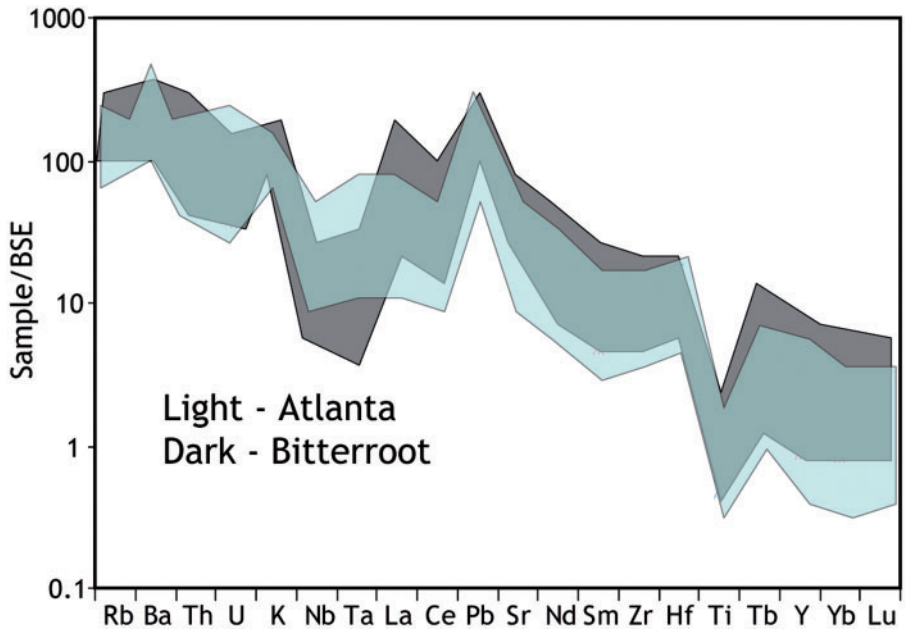

Fig. 4. Mantle-normalized trace element patterns for the Atlanta and Bitterroot peraluminous suites. Samples are normalized to Bulk Silicate Earth (BSE) after McDonough & Sun (1995).

plutons, and the lack of systematic increase in $^{208}Pb/^{204}Pb$ of the southern Challis plutons and Atlanta peraluminous suite with increasing $^{206}Pb/^{204}Pb$.

Zircon Hf isotopes

Representative zircon cathodoluminescence images are shown in Fig. 9. Despite considerable within-sample variability, zircon Hf isotopic results (Fig. 10) show a consistent decrease in ε_{Hf} values with time prior to Challis magmatism, essentially mirroring the trend of the whole-rock Nd and whole-rock Hf isotope data (Fig. 7). The oldest portion of the Idaho batholith, the early metaluminous suite, varies between −6 and −12. Internal variation is limited within single samples, and the coeval border zone suite has a similar range of ε_{Hf} values. The Atlanta peraluminous suite has considerably greater variation, both within and between samples. Inter-sample variation is generally correlated with age; the older samples of the suite range between −10 and −15 and youngest samples have values well below −15. For the late metaluminous suite, two samples from a large quartz diorite pluton in the western portion of the suite yield values between −10 and −15 whereas a sample from the northeastern part of the suite gave lower values from −15 to −20. The Bitterroot peraluminous suite shows a range of ε_{Hf} values primarily between −16 and −24, with only a few outliers. Samples from the Challis intrusions exhibit a huge overall range from 0 to −30 epsilon units, with the highest values coming from northern (45°N latitude) plutons and the lowest coming from southern (south of the latitude of Stanley) plutons. The Challis plutons also exhibit the most extreme case of within-sample variation, with sample 98IB6l ranging from −6 to −19. Although the inherent resolution of the laser ablation Hf method is relatively coarse (±2 ε units), the within-sample variation seen in 98IB6l and some other samples is far too large to be an artefact and instead probably reflects dynamic magmatic processes, such as magma mixing.

DISCUSSION

Overview

The Idaho batholith and Challis intrusive province represent a record of magmatism some 60 Myr long and demonstrate clear shifts in bulk composition and isotopic signature with time, reflecting changes in the relative importance of mantle input versus crustal melting. The striking shift in Nd and Hf (both zircon and whole-rock) isotopes (Figs 7 and 10) in the Idaho batholith magmatism to less radiogenic values with time, coincident with changes in major element compositions (Fig. 3), suggests that as magmatism progressed, the proportion of crustal melt involved in its petrogenesis, relative to mantle input, steadily increased with time until the onset of Challis magmatism. In addition, isotopic and trace element data suggest that different crustal lithologies at varying depths were melted as magmatism progressed. The higher average and maximum La/Yb and Sr/Y (Fig. 5b and c) values of the peraluminous suites suggest melting in the garnet stability field (i.e. at higher pressures) during the production

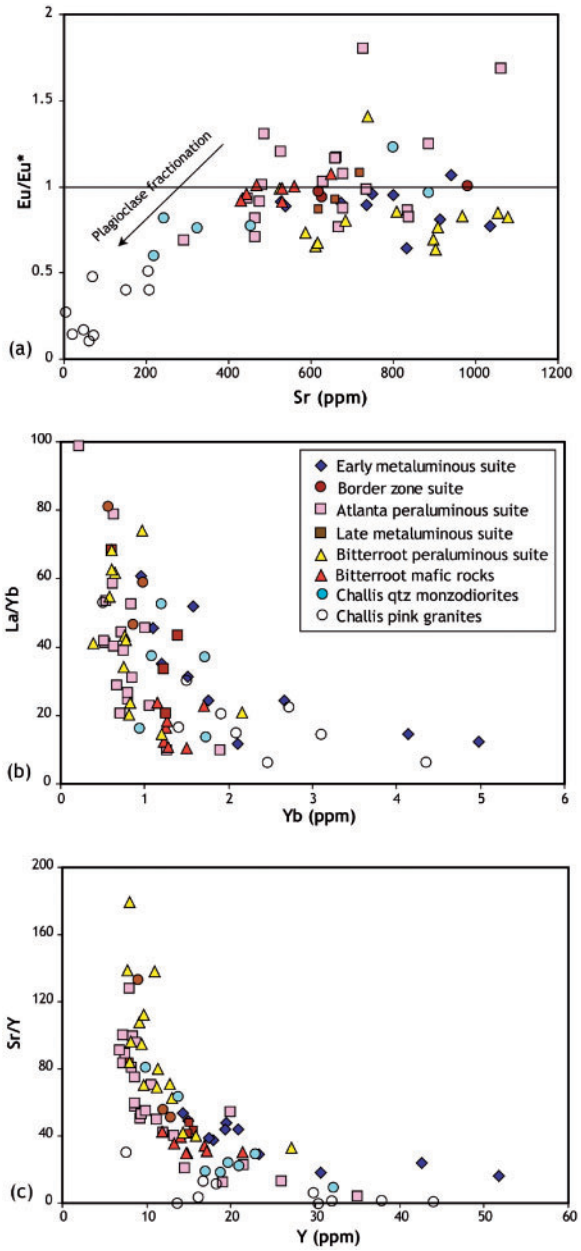

Fig. 5. Selected trace element characteristics of the Idaho batholith and Challis samples. (a) Eu/Eu* vs Sr; (b) La/Yb vs Yb; (c) Sr/Y vs Y.

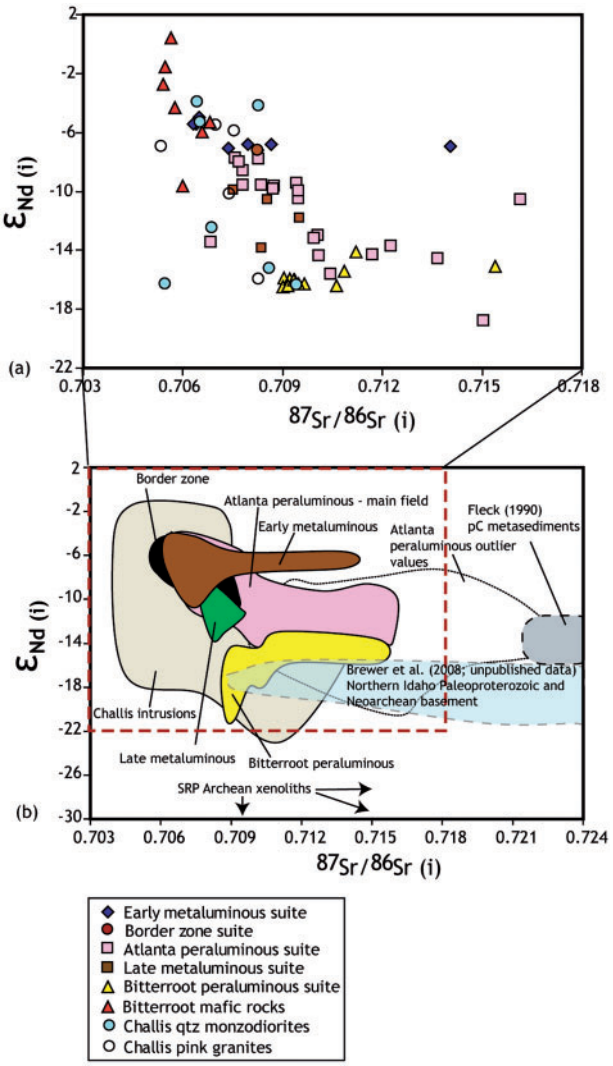

Fig. 6. Variation of ε_{Nd} (initial) vs $^{87}Sr/^{86}Sr$ (initial) for the Idaho batholith and Challis samples. (a) New data, this study. (b) Compiled data from the literature and this study for the Idaho batholith and Challis intrusions and potential crustal sources. (Note the expanded scale.) The shaded field for the Atlanta peraluminous suite represents the majority of analyses, whereas the dotted line encompasses outliers. Archean crustal xenoliths exhumed by Snake River Plain lavas (Leeman *et al.*, 1985) plot at lower ε_{Nd} and similar to higher $^{87}Sr/^{86}Sr$ values compared with those shown here.

of the peraluminous granitoids (e.g. Patiño Douce & Beard, 1995). In contrast, the low La/Yb and Sr/Y (Fig. 5b and c), negative Eu anomalies (Fig. 5a), and potassic nature (Fig. 3c) of the Challis rocks can be attributed to a combination of shallower melting and subsequent fractional crystallization in the plagioclase stability field (Norman *et al.*, 1992; Patiño Douce, 1999).

Potential crustal sources

The batholith is bordered to the north and south by Archean crustal blocks known from rare surface exposures and xenoliths (Leeman *et al.*, 1985; Doughty *et al.*, 1998; Wolf *et al.*, 2005); however, the basement age of the region intruded by the batholith is poorly known. Foster *et al.* (2006) have suggested that this region is composed primarily of Paleoproterozoic crust in what they referred to as the Selway terrane. Orthogneisses of 1·86 Ga age are known east of the Bitterroot lobe in Montana (Foster *et al.*, 2006), and Paleoproterozoic and Neoarchean crystalline rocks are now known in a high-grade terrane north of the Bitterroot lobe, containing 1·86 and 2·66 Ga

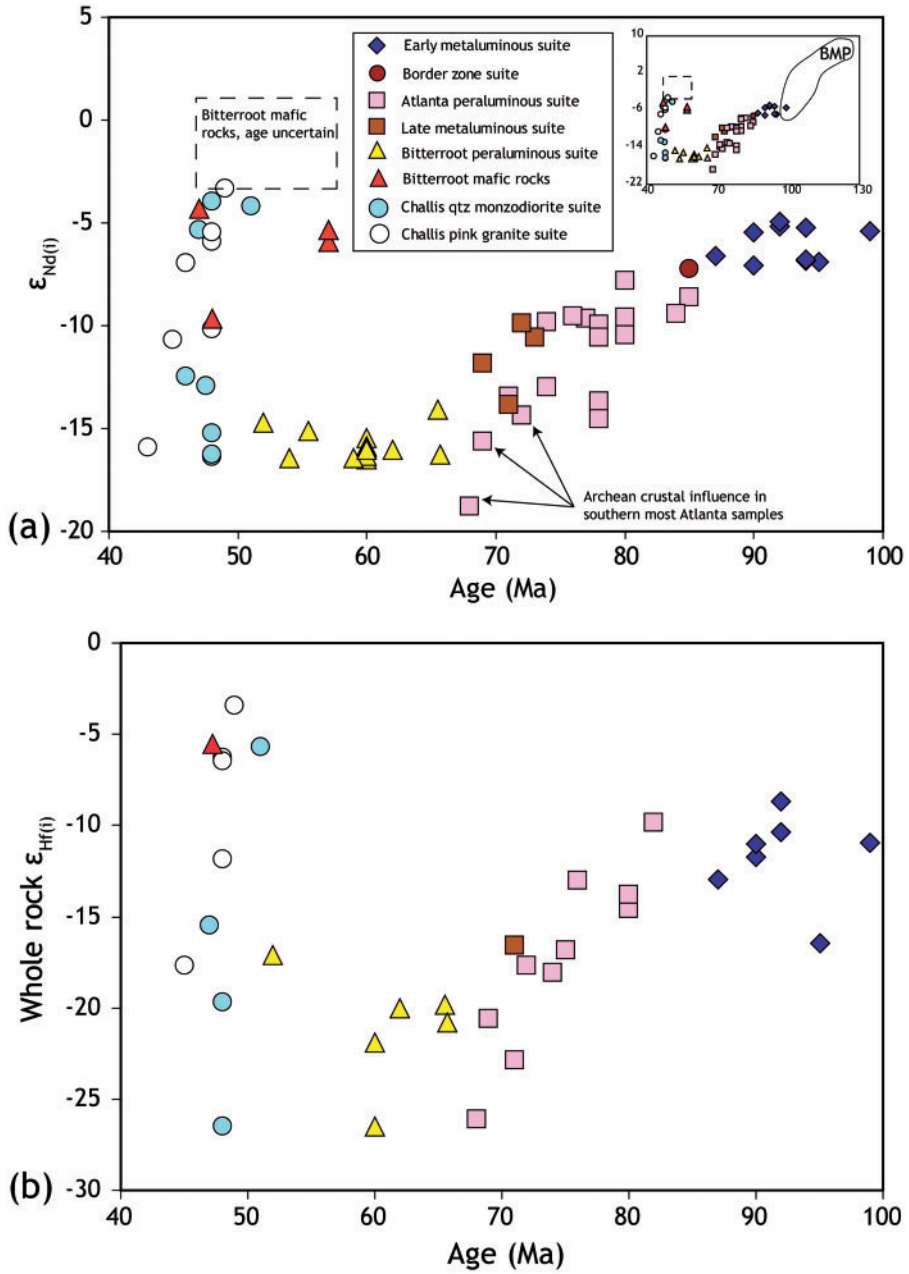

Fig. 7. (a) Variation of ε_{Nd} (initial) vs age. Because the age of some of the Bitterroot mafic samples is unclear, we show them as a field extending between 58 and 48 Ma. The inset shows the full range of Idaho batholith and Challis variation compared with the isotopically juvenile Early Cretaceous plutons in the eastern Blue Mountains province and Salmon River suture zone (Unruh *et al.*, 2008). These represent the ambient mantle whereas the Idaho batholith and Challis intrusions contain major crustal components. (b) Whole-rock ε_{Hf} (initial) vs age.

orthogneisses (Vervoort *et al.*, 2007; Brewer *et al.*, 2008) and 1·79 Ga anorthosites (Doughty & Chamberlain, 2007). This basement is overlain by Mesoproterozoic Belt Supergroup and Neoproterozoic Windermere metasedimentary rocks and, in southern Idaho, Paleozoic sedimentary rocks (e.g. Hyndman *et al.*, 1988; Lund *et al.*, 2003). Meta-igneous rocks of Mesoproterozoic, Neoproterozoic, Cambrian, and Ordovician age have also been recognized in the region of the Idaho batholith (Doughty & Chamberlain, 1996; Lund *et al.*, 2003, 2010; Alexander, 2007; Durk, 2007).

Origin of the early metaluminous and border zone suites

The compositionally diverse early metaluminous suite was constructed between 98 and 87 Ma, from mixtures of

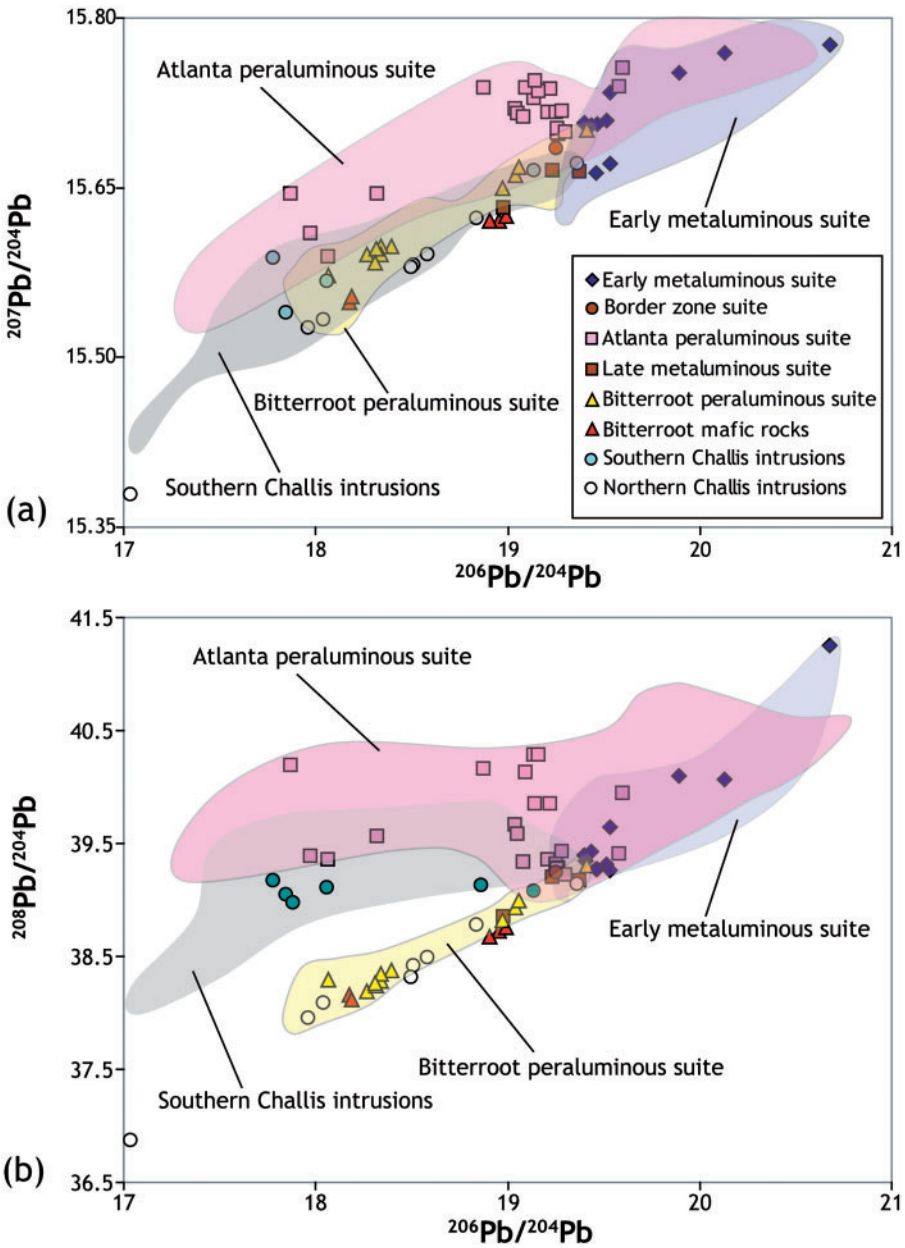

Fig. 8. Variation of $^{207}Pb/^{204}Pb$ vs $^{206}Pb/^{204}Pb$ (a) and $^{208}Pb/^{204}Pb$ vs $^{206}Pb/^{204}Pb$ (b) isotope plots. The fields include the new data from this study and previously published data from Shuster & Bickford (1985), Norman & Leeman (1989), Clarke (1990), Toth & Stacey (1992), Doe & Sanford (1995), Mitchell (1997), Reppe (1997), Robertson (1997), Panneerselvam *et al.* (2006), Unruh *et al.* (2008), and P. Larson (unpublished data) for the early metaluminous, Atlanta peraluminous, and Bitterroot peraluminous suites and the southern Challis intrusions. No older data exist for the other units.

mantle- and crustal-derived magmas produced by 'MASH'-like (mixing, assimilation, storage, and homogenization; Hildreth & Moorbath, 1988) or deep-crustal hot zone processes (Annen & Sparks, 2002). This origin is supported by the moderately radiogenic Sr and moderately unradiogenic Nd and Hf, which argue against pure melting of Precambrian crust, but highly radiogenic Pb and heavy oxygen isotopic compositions (Gaschnig *et al.*, 2008*b*), which require a supracrustal component (i.e. metasedimentary rocks). The results of melting experiments also support a hybrid origin for this suite, as it overlaps with compositions formed by the experimental interaction of arc basalt and metasedimentary rock (Fig. 11; Patiño Douce, 1999). The proportion of mantle to crustal input involved in the production of this suite, however, is difficult to determine because of the uncertain role

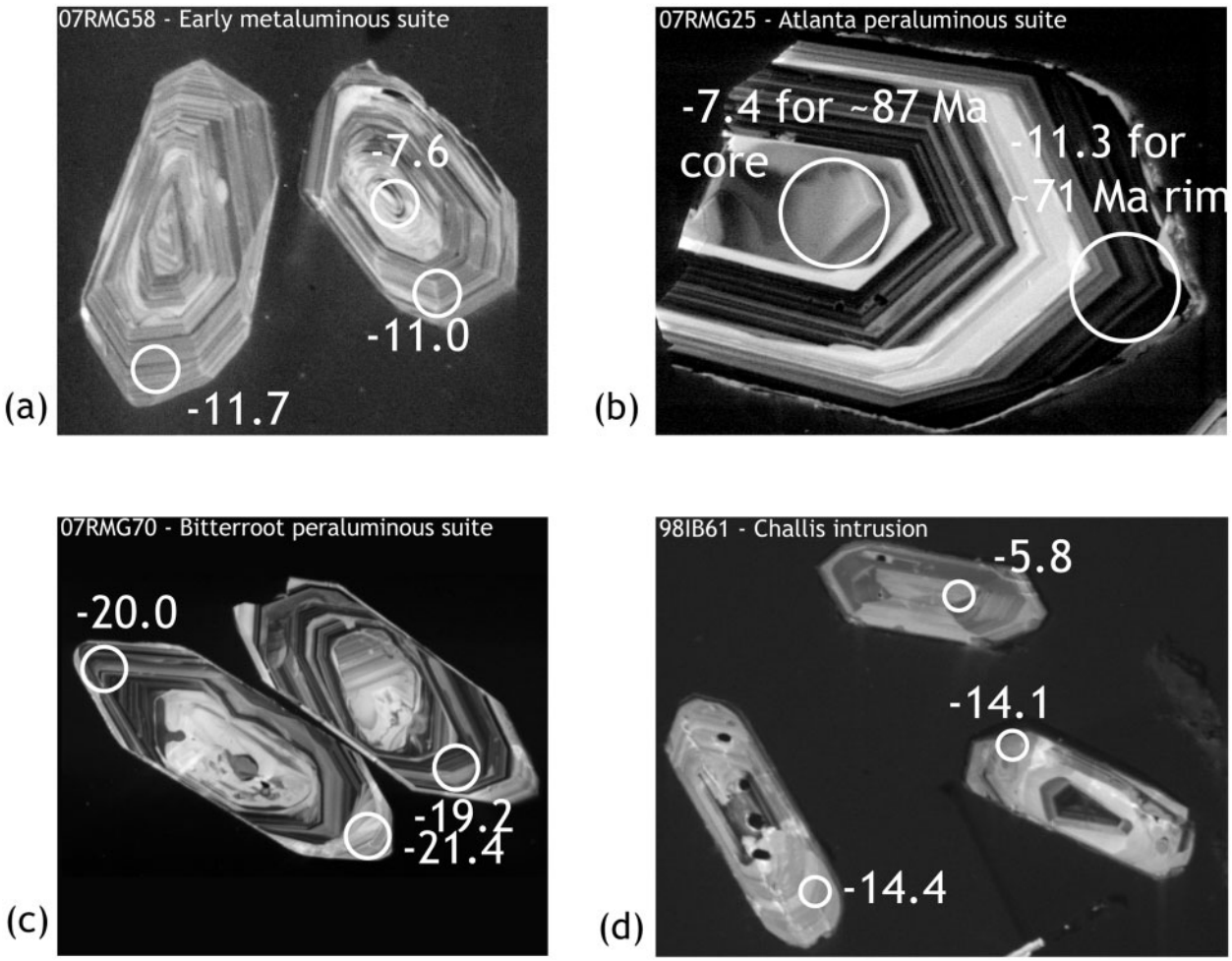

Fig. 9. Representative zircon cathodoluminescence images. Spots analyzed for Hf isotopes by LA-MC-ICP-MS with initial ε_{Hf} values are marked in white.

of the lithospheric mantle and the wide age range of sedimentary rock units (Mesoproterozoic to Late Paleozoic) in southern and central Idaho. For example, if we use Mesoproterozoic Belt Supergroup metasedimentary rocks (Frost & Winston, 1987) and average mantle-derived basalts (Kelemen *et al.*, 2003) as crust and mantle end-members, mixing calculations based on Nd isotopes suggest a crust–mantle ratio of about 35:65 to 25:75. Although Sr and Pb isotopes vary greatly in Belt Supergroup rocks (Shuster & Bickford, 1985; Criss & Fleck, 1987; Fleck, 1990; Fleck *et al.*, 2002), calculations based on these systems yield crust and mantle proportions similar to those from Nd isotopes. These estimates probably represent a lower limit in the amount of crust required because the use of less isotopically evolved Paleozoic sedimentary rocks (e.g. Boghossian *et al.*, 1996) would require greater relative crustal input.

The border zone suite is coeval with the early metaluminous suite, and their geochemical and isotopic compositions largely overlap. Based on the compositional similarities, we consider the border zone suite to be produced by the same crust–mantle hybridization processes as the early metaluminous suite, a model broadly similar to the one proposed by Manduca *et al.* (1992) for the border zone suite. We speculate that these suites may have originally formed a more continuous igneous complex, which either existed at a higher structural level than now exposed or was destroyed or obscured by the younger peraluminous phases of the batholith (Gaschnig *et al.*, 2010).

Origin of the Atlanta peraluminous suite

The voluminous Atlanta peraluminous suite was intruded between 83 and 67 Ma, and appears to be primarily the product of melting of a mixture of Neoproterozoic and Archean components in the lower crust with little input from the mantle. It has a very limited compositional range and is similar to melts derived by experimental biotite dehydration melting of 'metagreywacke' (Fig. 11;

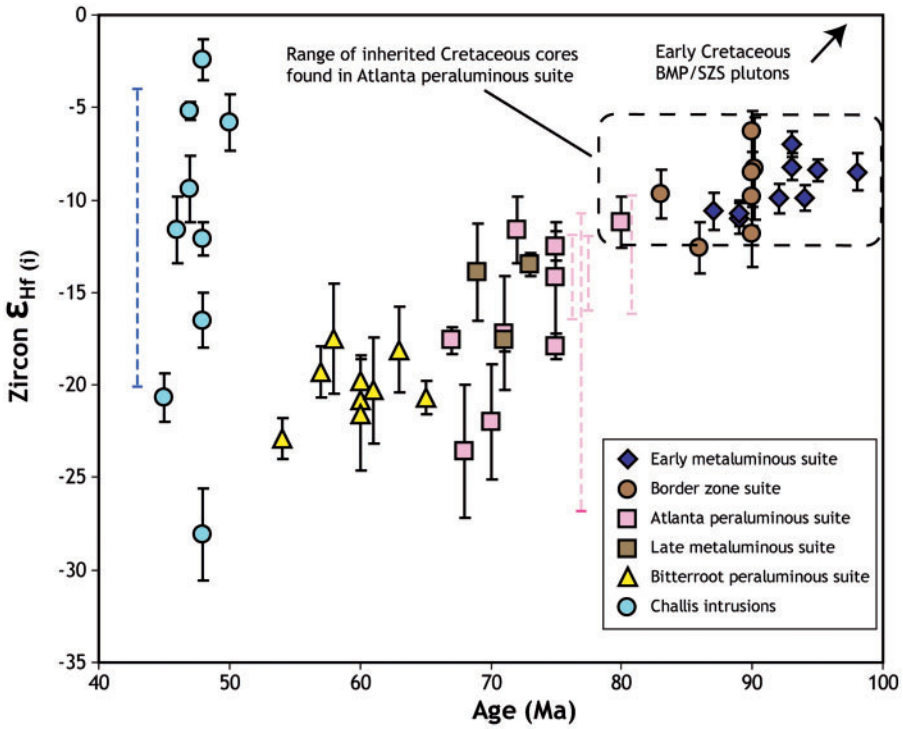

Fig. 10. *In situ* Hf isotope data from magmatic zircon rims vs age. The symbols represent weighted means and their uncertainties and are calculated from multiple spot analyses from single samples. Weighted mean values are shown only for samples where the individual analyses appear to be normally distributed. The dashed error bars that lack symbols represent the range in ε_{Hf} values for the samples that lacked normal distributions. Two of these samples, 98IB61 and 07RMG56, have extreme within-sample heterogeneity, spanning ~15 ε units. The dashed field represents the age and isotopic range of older Cretaceous cores found in Atlanta peraluminous suite zircons. Early Cretaceous plutons in and just west of the suture zone have highly juvenile zircon Hf isotopic compositions (S. Dufrane, unpublished data; arrow).

Patiño Douce, 1999), or biotite-bearing intermediate to felsic igneous rocks (e.g. Watkins *et al.*, 2007). These lines of evidence, coupled with the evolved Nd and Hf isotopes, support a largely crustal source. The major and trace element characteristics also indicate that melting occurred in the garnet stability field, most probably at ≥10 kbar, constraining melt formation to lower crustal depths of at least ~35 km (e.g. Patiño Douce & Beard, 1995). Although an origin of the 'garnet signature' by chemical inheritance from the melting protolith has been suggested (Moyen, 2009), only very large melt fractions will retain this signature, unless the protolith itself is melted in the garnet stability field.

Important constraints on the ages of the source lithologies come from zircon inheritance patterns (Gaschnig *et al.*, 2008*a*, in preparation), which show dominantly two age peaks in the Neoproterozoic and Neoarchean, both equivalent to exposed rocks in central and southern Idaho (Lund *et al.*, 2003; Alexander, 2007; Durk, 2007) and mid- to lower-crustal xenoliths from Snake River Plain lavas (Leeman *et al.*, 1985; Wolf *et al.*, 2005). The Archean inheritance pattern, less radiogenic Nd and Hf values, and higher $^{207}Pb/^{206}Pb$ indicate that the southern Atlanta peraluminous suite incorporated Archean crustal material that either is not present or is less important in granite petrogenesis further north. The interlayered Neoproterozoic and Archean ortho- and paragneisses that occur in the Pioneer and House Mountain complexes (Alexander, 2007; Durk, 2007; P. Link, personal communication, 2011) may be representative of the source region for the southern Atlanta peraluminous suite. To the north, the Archean component appears to vanish and the Neoproterozoic becomes more important. Few major and trace element data (Lund *et al.*, 2010) and no isotopic data exist in the literature for Neoproterozoic rocks in this region, making it difficult to assess quantitatively their petrological role. New Nd and Pb isotopic data presented here (Supplementary Data Appendix D) on two Neoproterozoic metavolcanic samples are consistent with mixing of Neoproterozoic and Archean components (Fig. 12). These data can explain the unusual positive correlation between ε_{Nd} and $^{206}Pb/^{204}Pb$ (Fig. 12), representing a mixing array between the strongly unradiogenic Pb and Nd of the Archean crust with more radiogenic Pb and Nd of the Neoproterozoic crust. Simple mixing of a crust and mantle component would produce a data array orthogonal to this trend, and realistic

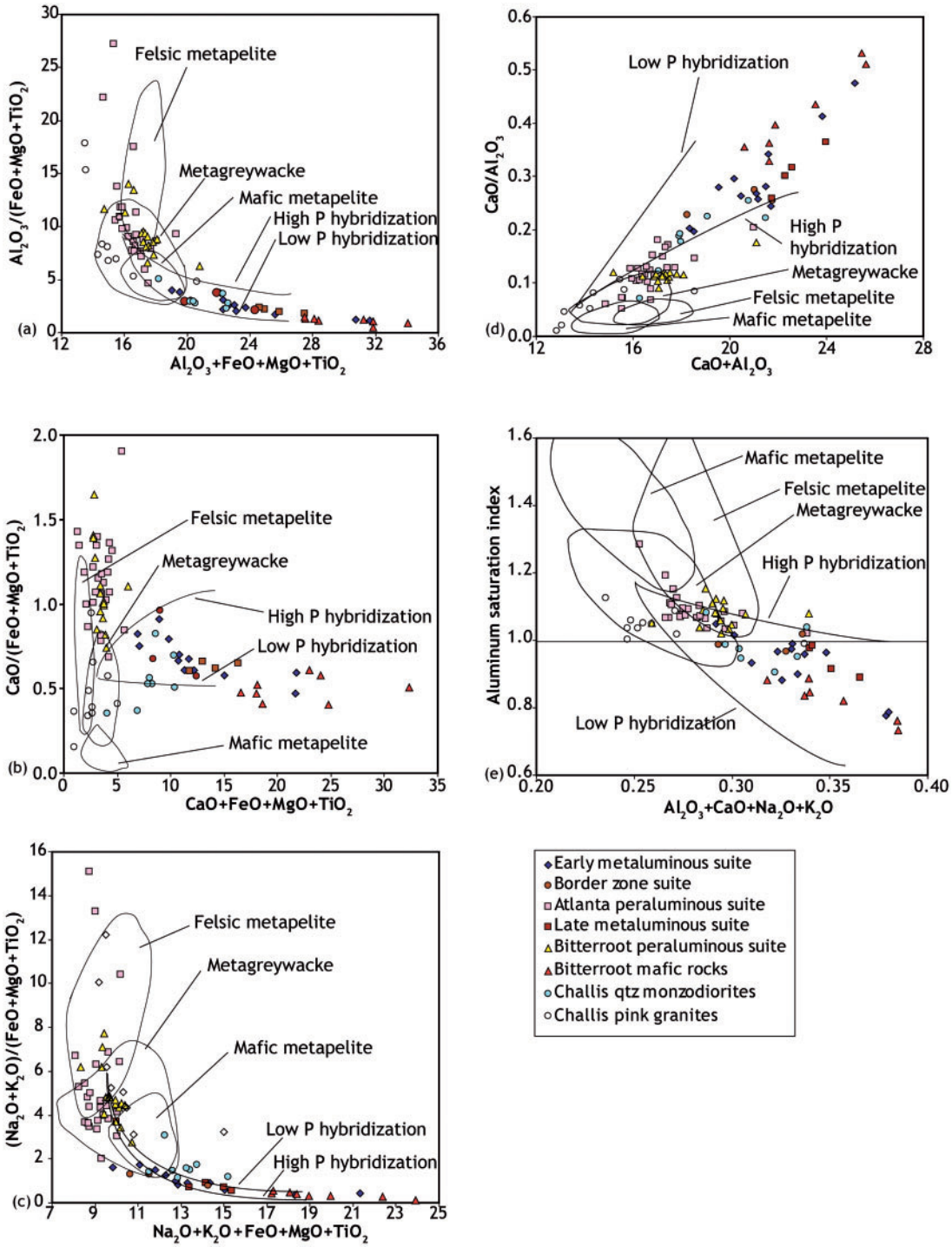

Fig. 11. Comparison of the compositions of the Idaho batholith and Challis intrusions with experimentally produced melts. Fields and discriminant schemes are from Patiño Douce (1999). 'Hybrid' curves represent trajectories created by the experimental interaction of arc basalt with metagreywacke at different pressures. It should be noted that the early metaluminous, border zone, and late metaluminous suites, Bitterroot mafic rocks, and some Challis intrusions plot along the hybrid curves, whereas the two peraluminous suites primarily plot within the metagreywacke field. One discrepancy between the peraluminous suites and metagreywacke melts is the slightly higher CaO and lower $FeO + MgO + TiO_2$ of the peraluminous suites.

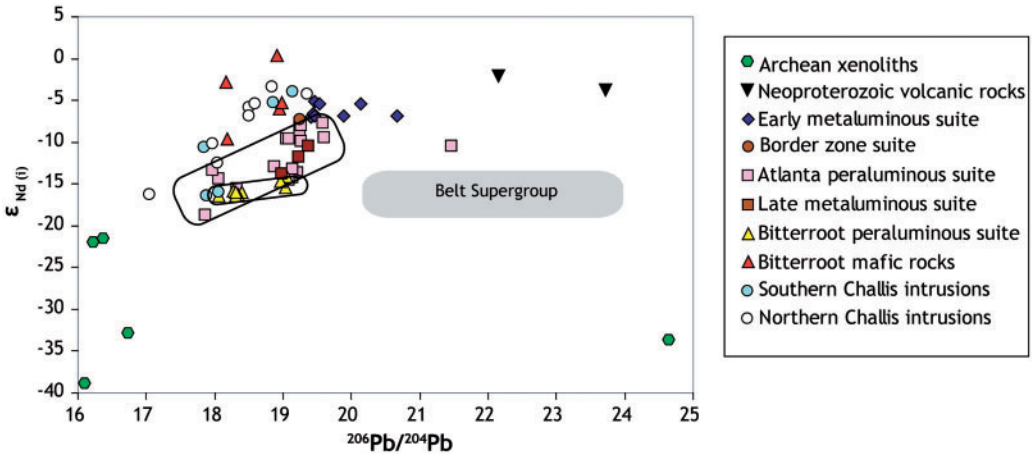

Fig. 12. Variation of ε_{Nd} vs $^{206}Pb/^{204}Pb$ for the Idaho batholith and Challis intrusions compared with regional crustal rocks. Data sources for crustal rocks: Neoproterozoic volcanic rocks from this study; Archaean crustal xenolith data from Leeman *et al.* (1985); Belt Supergroup field from Shuster & Bickford (1985), Frost & Winston (1987) and Panneerselvam *et al.* (2006).

assimilation–fractional crystallization (AFC) models for crust–mantle interaction also fail to reproduce the observed trend. In addition, limited trace element data for the central Idaho metavolcanic and plutonic rocks (Lund *et al.*, 2010) show that these rocks are enriched in HFSE and lack Nb–Ta depletion. The Atlanta peraluminous rocks also lack Nb–Ta depletion (Fig. 4), which may indicate that this characteristic was inherited from the Neoproterozoic source material.

Some inherited zircons observed in the Atlanta peraluminous suite are only 5–20 Myr older than the host magma (Gaschnig *et al.*, 2010). These xenocrysts are similar in age to the early metaluminous and border zone suites, and they occur as cores, with typically narrower magmatic rims, and as rare whole crystals, suggesting that they were picked up relatively late in the history of the magma. Because plutons of the early metaluminous suite occur as roof pendants in parts of the Atlanta peraluminous suite, it is conceivable that some of these older rocks were assimilated at or near the level of emplacement of the Atlanta peraluminous magmas, accounting for the Cretaceous inheritance. The comparatively small isotopic contrast between the two suites makes assimilation of the early metaluminous suite otherwise difficult to detect.

The evidence presented here provides little doubt that the Atlanta peraluminous magmas contained a large portion of melted Precambrian crust. It is more difficult, however, to ascertain if these were 100% crustal melts with only heat input (i.e. no mass transfer) from mantle-derived basalts to trigger crustal melting. Although limited overlap into the hybrids fields in Fig. 11 and the more calcic nature of the Atlanta peraluminous suite (Fig. 11b and d) can be used to argue for some level of mantle basalt input, the limited compositional range, lack of correlation between bulk-rock and isotopic composition, and lack of contemporaneous mafic rocks suggest that any input was probably small.

Origin of the late metaluminous suite

The limited amount of available data makes it difficult to draw firm conclusions about the origin of the late metaluminous suite, which forms a belt of small plutons around the Bitterroot lobe of the Idaho batholith. The mafic to intermediate nature of the rocks and similarity to experimental melts of arc basalt mixed with metasedimentary rock (Patiño Douce, 1999; Fig. 11) suggest that they are unlikely to be pure crustal melts and probably are hybrids. More data are clearly needed to develop and test any model for the origin of these rocks.

Origin of the Bitterroot peraluminous suite (and associated Bitterroot mafic rocks)

The Bitterroot peraluminous suite formed between 66 and 54 Ma. It has a narrow major element compositional range, similar to that of the Atlanta peraluminous suite, which overlaps with experimentally produced melts of metagreywacke (or intermediate to felsic meta-igneous rocks; Fig. 11). Conversely, the subtle trace element differences (Fig. 4) and strong differences in Nd, Hf, and Pb isotopic compositions (Figs 6, 7, 8 and 10) require a different source for the Bitterroot peraluminous suite.

We propose instead that the Bitterroot peraluminous suite is largely derived from partial melting of Paleoproterozoic and Neoarchean basement orthogneisses in northern Idaho (Vervoort *et al.*, 2007; Brewer *et al.*, 2008) and western Montana (Foster *et al.*, 2006), an idea first suggested by Mueller *et al.* (1995) before the identity of the orthogneisses was known. These rocks appear to overlap the Bitterroot peraluminous suite in Sr and Nd isotopic composition, based on the limited available data

(Brewer *et al.*, 2008; unpublished data). At the present level of exposure in the drainage of the North Fork of the Clearwater River (~100 km NE of Lewiston; Fig. 1), these basement rocks have been subjected to amphibolite-grade metamorphism and local migmatization. As in the case of the Atlanta peraluminous suite, dehydration melting of these rocks at greater pressures in the garnet stability field should yield melts with major and trace element characteristics similar to those seen in the Bitterroot peraluminous suite. The weak negative Eu anomaly decoupled from Sr concentration (i.e. not linked to residual or fractionating plagioclase) may be inherited from this source or gained from subsequent assimilation (see below; Fig. 5a).

One key problem with Paleoproterozoic basement as the sole source of the Bitterroot peraluminous suite is the continuous nature of its inherited zircon age spectrum between 1900 and 1300 Ma (Foster & Fanning, 1997; Gaschnig *et al.*, 2008*a*, in preparation). The similarity of the zircon inheritance to the detrital zircon age spectra of the Belt Supergroup (Ross & Villeneuve, 2003; Lewis *et al.*, 2007*b*; Link *et al.*, 2007) suggests that Belt rocks were incorporated into the Bitterroot peraluminous magmas. The Nd isotopic composition of the Belt Supergroup (Frost & Winston, 1987; Fleck, 1990) overlaps with the Bitterroot peraluminous suite; however, the Belt has an extremely radiogenic Sr isotopic signature (modern $^{87}Sr/^{86}Sr$ often >0·8; Criss & Fleck, 1987; Fleck, 1990; Fleck *et al.*, 2002). The low Sr concentration in Belt rocks (typically less than 200 ppm; Criss & Fleck, 1987; Lewis & Frost, 2005) compared with the high Sr concentration of the Bitterroot peraluminous suite (up to 1000 ppm), however, means that Belt rocks will exert very little leverage on the Sr isotopic budget. This observation, along with oxygen isotope constraints (Fleck & Criss, 1985; King & Valley, 2001), allows the Bitterroot peraluminous suite to contain up to 10% Belt component. These Belt rocks may have melted together with the basement orthogneisses in the source region, which is plausible given the juxtaposition of the two rock types on the northern margin of the Bitterroot lobe. This is also an appealing scenario as mixed rocks have been shown experimentally to have greater melt fertility than the separate lithologies alone (Skjerlie *et al.*, 1993; Skjerlie & Patiño Douce, 1995). Alternatively, the Belt rocks may have been assimilated at or near the level of emplacement.

The significance of the Bitterroot mafic rocks to the petrogenesis of the Bitterroot peraluminous suite is unclear (Foster & Hyndman, 1990). Foster & Fanning (1997) and Gaschnig *et al.* (2010) have published Paleocene and Eocene ages, respectively, for different localities. Some mafic rocks, but not all, are contemporaneous with the later stages of Bitterroot peraluminous magmatism. The large isotopic contrast between the mafic rocks and their granite hosts (Figs 6 and 7) and lack of transitional compositions, however, argue that the role of magma mixing in the petrogenesis of the Bitterroot peraluminous suite is insignificant. In addition, field evidence suggests that the mafic magmas were injected late in the crystallization history of the granites (Foster & Hyndman, 1990). The mafic magmas themselves are chemically analogous to continental arc basalts and probably trace their lineage to mantle-derived melts (Hyndman & Foster, 1988).

Origin of the Challis intrusions

Rocks of the Challis intrusive province and volcanic field exhibit a wide range of compositional and isotopic diversity. Our data are generally consistent with previous interpretations that these magmas have diverse origins ranging from nearly pure crustal melts to only slightly contaminated lithospheric mantle-derived melts (Clarke, 1990; Norman & Mertzman, 1991; Larson & Geist, 1995; Mitchell, 1997; Reppe, 1997; Robertson, 1997; McKervey, 1998). The relatively potassic nature (Fig. 3c) of the Challis rocks, coupled with their high Rb/Sr and large negative Eu anomalies (especially common in the pink granites) (Fig. 5a), suggests a major role for plagioclase as a residual and/or fractionating phase, requiring formation or at least residence at lower pressures than the two peraluminous suites (Norman *et al.*, 1992). Our new isotopic data show a contrast between Challis plutons in southern Idaho (where all of the studies mentioned above were focused) and northern Idaho (north of ~45°N). Relatively radiogenic Nd and Hf isotopic compositions are more prevalent in the northern Challis plutons and do not match any known crustal source. These plutons also form a distinct array in Pb isotopic space that closely parallels the Bitterroot peraluminous suite, which many of them intrude. Consequently, the input of a mantle-derived component may be greater in the northern Challis plutons compared with those in the south, possibly owing to the greater amount of extension associated with the Bitterroot metamorphic core complex.

Crustal growth or recycling?

It is clear from the evidence presented here that all components of the Idaho batholith and Challis intrusive province contain a significant quantity of pre-existing crust and none represent purely juvenile melts from the mantle. The relative contributions from the mantle and crust, however, have clearly changed with time. Juvenile input is most evident in (1) the early metaluminous, border zone, and possibly late metaluminous suites; (2) the Bitterroot mafic rocks; and (3) some of the Challis intrusive rocks. The ratios of crust to mantle inputs are, however, difficult to quantify because of the wide range of possible crustal end-members, lack of their isotopic characterization, and the uncertain role of melts derived from the lithospheric mantle. The peraluminous suites appear to have formed predominantly from melting of pre-existing crust; if they

contain a mantle-derived component, its chemical fingerprint is cryptic. These suites make up 59% by areal extent (81% if the Challis is excluded) of the currently exposed ~32 000 km^2 system and imply that the magmatism was dominated by crustal recycling with little new crustal growth. It should be kept in mind, however, that the early metaluminous and border zone suites, which have a clear juvenile mantle contribution, appear to be the preserved remnants of a much larger igneous system that once occupied most of the present-day footprint of the batholith (see above; Gaschnig *et al.*, 2010). If this hypothesis is correct, the Idaho batholith and Challis systems may have been more important as centers of crustal growth than otherwise thought.

Tectonic implications

The data presented here, together with previous studies of the Idaho batholith, allow us to provide constraints on the tectonic environment in which the Idaho batholith and Challis intrusive province formed. The geochemical and geochronological constraints are as follows.

(1) Following the accretion of the Blue Mountains Province and sporadic mid-Cretaceous juvenile magmatism within the province and Salmon River suture zone, the earliest phase of Idaho batholith magmatism occurred from 98 to 87 Ma. This magmatism is represented by the early metaluminous and border zone suites on the east and west sides of the Atlanta lobe, respectively. These suites have mixed crust–mantle isotopic signatures and are compositionally similar to the plutons of the Cretaceous Sierra Nevada batholith.

(2) The Atlanta peraluminous suite, the largest single component of the batholith based on present-day outcrop patterns, formed between 83 and 67 Ma. This suite formed dominantly through crustal melting at ≥10 kbar pressure. Nd, Hf, and Pb isotope data and evidence for zircon inheritance suggest involvement of a significant Archean crustal component in the generation of the southern Atlanta peraluminous suite, whereas Neoproterozoic crustal units were more important in the northern Atlanta peraluminous suite.

(3) Starting at around 70 Ma, a more localized episode of magmatism began in northern Idaho, with emplacement of small mafic to intermediate plutons of the late metaluminous suite, followed by the larger Bitterroot peraluminous suite between 66 and 54 Ma. The younger Bitterroot peraluminous suite, although compositionally and petrographically similar to the Atlanta peraluminous suite, has a distinctly different isotopic composition, and was generated through the melting of different crustal sources, most probably a mixture of Neoarchean to Paleoproterozoic basement and Mesoproterozoic metasedimentary rocks.

(4) The 51–43 Ma Challis intrusive province is compositionally and isotopically diverse and cuts all older magmatic suites. The Nd and Hf isotopic data for the Challis require a significant mantle contribution for many of these rocks.

Based on the above constraints, we suggest the following tectonic model for the Idaho batholith–Challis system (Fig. 13). Early metaluminous and border zone suite magmatism occurred at the same time as voluminous magmatism throughout the western USA (a magmatic flare-up; e.g. Ducea & Barton, 2007). The age, geochemistry, and mixed crust–mantle isotopic signatures of the early metaluminous and border zone suites are similar to those of the Cretaceous Sierra Nevada and Peninsular Ranges batholiths. This, in conjunction with recent recognition of plutons of similar age and composition in northwestern Nevada (Van Buer & Miller, 2010), suggests that a continuous continental arc batholith existed in the Late Cretaceous from Baja California to at least as far north as the present-day Canadian border. It should be noted, however, that at the latitude of the Idaho batholith, this arc magmatism was accompanied by intense deformation in the western Idaho shear zone (Giorgis *et al.*, 2008).

At around 85 Ma, arc magmatism in the Sierra Nevada and Peninsular Ranges ceased (Bateman, 1992; Coleman & Glazner, 1997; Ortega-Rivera *et al.*, 1997; Ortega-Rivera, 2003; Saleeby *et al.*, 2008); however, the Idaho batholith continued to be active, with a voluminous episode of predominantly crustal melting between 83 and 67 Ma. We attribute the crustal melting to crustal thickening, which is documented both locally (Silverberg, 1990; Foster *et al.*, 2001; Alexander, 2007; Lund *et al.*, 2008; Dye *et al.*, 2009) and regionally (e.g. DeCelles, 2004; Wells *et al.*, 2009) for this interval. The cause of crustal thickening is less clear and we outline two possible scenarios below.

After the formation of the Atlanta peraluminous suite, a second more localized (between ~45·8° and 46·8°N) episode of crustal melting occurred between 66 and 54 Ma, leading to the formation of the Bitterroot peraluminous suite. This second crustal melting event is attributed to localized crustal thickening, supported by evidence of metamorphism in the vicinity of the Bitterroot lobe at ~60 Ma (House *et al.*, 1997; Doughty *et al.*, 2007; Lund *et al.*, 2008), transpressional deformation along the Orofino shear zone (McClelland & Oldow, 2007), and formation of the Coolwater culmination (Lund *et al.*, 2008). The local emplacement of some of the Bitterroot mafic rocks at 56·5 Ma may record the first indication of extension in the over-thickened crust, which ultimately led to the exhumation of the Bitterroot metamorphic core complex several million years later (Foster & Fanning, 1997; Foster *et al.*, 2001).

The subsequent Challis magmatic event reflects a major regional shift to extensional tectonics in the northern Cordillera (e.g. Armstrong & Ward, 1991). The generation of associated Eocene magmatism has been attributed to

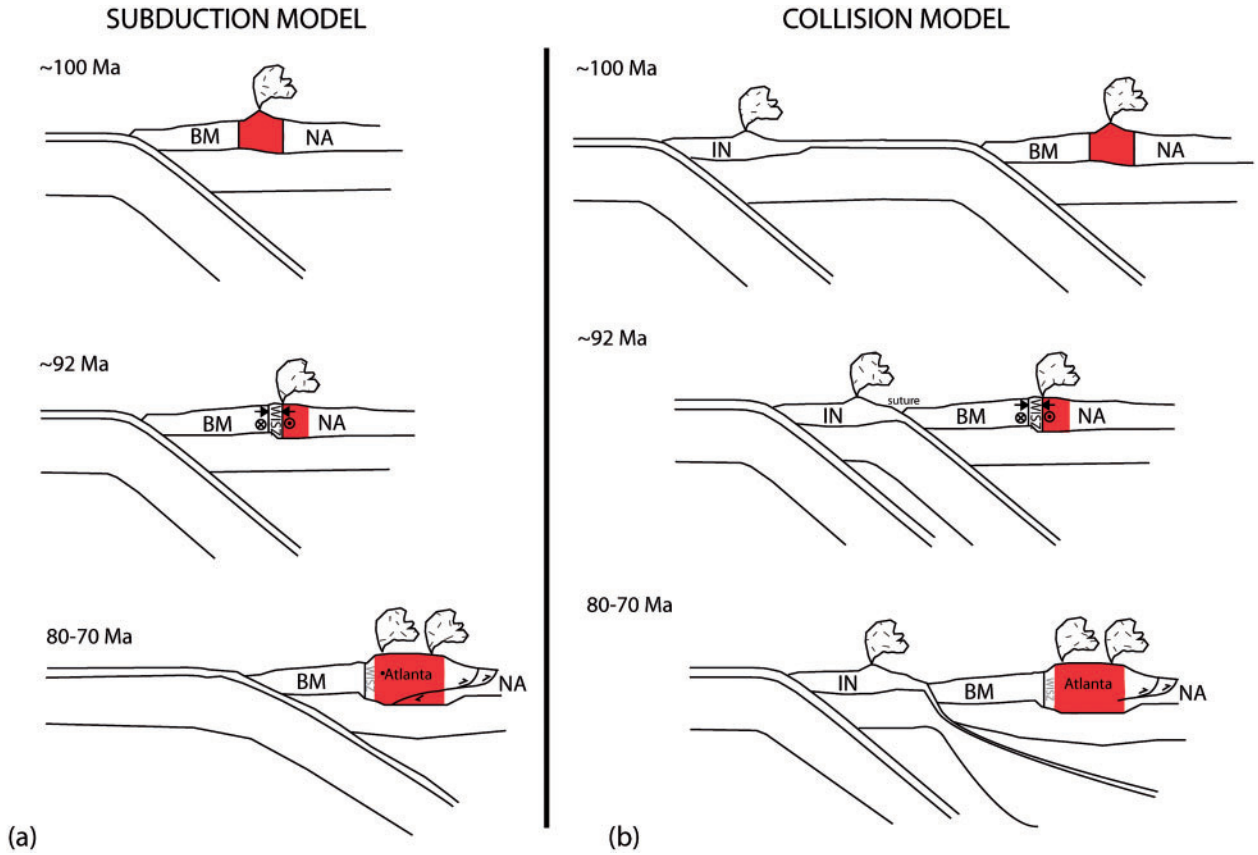

Fig. 13. Schematic tectonic cross-sections showing two models, (a) subduction and (b) collision, for the ~100 to 70 Ma magmatism of the Idaho batholith. Both models begin with the waning of magmatism in the suture zone suite at 100 Ma. At ~92 Ma, considerable shortening of the suture zone rocks by the western Idaho shear zone (WISZ) occurred because of continued subduction or the collision of an outboard terrane. Continuing arc magmatism occurred during this time inboard of the WISZ, recorded by the early metaluminous and border zone suites. Between 80 and 70 Ma, thickening and melting of North American crust produced the Atlanta peraluminous suite. Crustal thickening could have resulted from a change in the convergence rate and/or slab dip at the subduction zone (subduction model) or from shortening associated with continued terrane collision (collision model). BM, Blue Mountains province; NA, North America; IN, Insular Superterrane.

different mechanisms: decrease in the rate of plate convergence at the western North American margin (Constenius, 1996); opening of a slab window, as a result of either ridge subduction (Breitsprecher *et al.*, 2003; Haeussler *et al.*, 2003; Madsen *et al.*, 2006; Duke, 2009) or 'sideways' slab rollback (Humphreys, 1995). All of the Eocene magmatism appears to have been driven by mantle melting, possibly with a strong lithospheric mantle component (e.g. Dudas *et al.*, 1987; O'Brien *et al.*, 1995; McKervey, 1998; Feeley, 2003; Duke, 2005). In the case of Challis rocks in Idaho, the lithospheric mantle may have melted (Norman & Mertzman, 1991; McKervey, 1998), although it is unclear whether melting was due to decompression associated with extension or the influx of hot asthenosphere. In any case, the mantle melts that infiltrated the crust triggered crustal melting by providing heat and also mixed with some of these crustal melts.

Two models for Late Cretaceous crustal melting and thickening

An important unanswered question is what processes led to the widespread crustal thickening and subsequent crustal melting that produced the voluminous Atlanta peraluminous magmatism, which forms the majority of the present-day exposure of the Idaho batholith (Fig. 13).

If the subduction setting that produced the early metaluminous and border zone suites continued after ~85 Ma, thickening may have occurred as a result of changes in the rate and angle of convergence at the plate boundary (e.g. Engebretson *et al.*, 1984; Stock & Molnar, 1988) (Fig. 13a). To explain the lack of a recognizable mantle signature within the granitic intrusions in this scenario, the subduction-related basalts would pool at the Moho or in the lowermost crust and provide heat for crustal melting but not directly interact with the resulting crustal melts.

This scenario has some broad similarities to the models of Ducea (2001) and Ducea & Barton (2007) for high magmatic flux episodes in the other Cordilleran batholiths.

An alternative explanation (Fig. 13b) for the cause of crustal melting is the collision of allochthonous terranes outboard of the Blue Mountains province. This scenario takes into account evidence based on paleomagnetism (e.g. Irving, 1985; Mahoney *et al.*, 2000; Haggart *et al.*, 2006) and regional fault reconstructions (Wyld *et al.*, 2006) for a Late Cretaceous northward translation of the Insular Superterrane, which is the most outboard terrane in the Canadian Cordillera. In this model, the outboard terrane collides with western North America at middle latitudes between 100 and 90 Ma and is then translated hundreds to thousands of kilometers to the north (Maxson & Tikoff, 1996; Umhoefer *et al.*, 2006). Deformation from the collision is initially focused along the western Idaho shear zone (Giorgis *et al.*, 2008), but gradually leads to the large-scale thickening of adjacent North American lithosphere and crustal melting leading to the formation of the Atlanta peraluminous suite.

CONCLUSIONS

The Idaho batholith records a long history of magmatism, characterized by significant crustal recycling, coupled with juvenile, mantle-derived input during certain intervals. The initial magmatism of the early metaluminous and border zone suites (~100 to 87 Ma) contained both crust and mantle components and probably occurred in a typical arc environment similar to that of the other Cordilleran batholiths. These suites and the slightly older adjacent plutons were originally extensively distributed but were obliterated by younger plutonism and dramatically shortened in the western Idaho shear zone, respectively. Voluminous magmatism of the Atlanta peraluminous suite occurred from 83 to 67 Ma. This is thought to have been derived dominantly by crustal melting with little direct mantle input, related to crustal thickening either in a continued subduction environment or after the collision of an outboard terrane. At ~70 Ma, a volumetrically minor magmatic episode occurred in the northern portion of the batholith and produced the late metaluminous suite, followed by renewed crustal melting between 66 and 54 Ma, creating the Bitteroot peraluminous suite. The Bitterroot peraluminous suite, although of similar bulk composition, is isotopically distinct from the Atlanta peraluminous suite, indicating different crustal sources. Finally, the Eocene Challis magmatic event occurred after a switch to extensional tectonics and involved both mantle-derived magmatism and crustal recycling.

The ~45 Myr records of magmatism of the Idaho batholith and Challis intrusive province are the results of the two competing tectonic processes of crustal thickening and extension, which controlled the contributions of juvenile mantle-derived basalts and the degree and depth of crustal melting. Differences in basement age and composition resulted in geographical isotopic variations both within and between magmatic suites. Thus, the formation of the Idaho batholith and Challis intrusive province reflects the influence of both external tectonic forcing and pre-existing lithospheric composition and architecture.

ACKNOWLEDGEMENTS

We thank John Valley and Elizabeth King for zircon separates and rock powders; Bill McClelland, Karen Lund, and John Aleinikoff for zircon separates; and Garret Hart, Andy Dufrane, Robbie King, Charles Knaack, and Rick Conrey for analytical help. We thank Tony Kemp and Peter Larson for helpful discussions and informal reviews. We thank Mark Schmitz, Tom Frost, and Dave Foster for helpful and constructive reviews, and Ron Frost for editorial handling.

FUNDING

This work was supported by National Science Foundation grants EAR-0844149 and EAR-0537913 to J.D.V., EAR-0844260 to B.T., a GSA Graduate Student Research Grant, and a Praetorius-Exxon Graduate Fellowship.

SUPPLEMENTARY DATA

Supplementary data for this paper are available at *Journal of Petrology* online.

REFERENCES

Alexander, J. T. (2007). Geochronology of the House Mountain gneiss complex in the Atlanta lobe of the Idaho batholith. MS thesis, Boise State University, Boise.

Annen, C. & Sparks, R. S. J. (2002). Effects of repetitive emplacement of basaltic intrusions on thermal evolution and melt generation in the crust. *Earth and Planetary Science Letters* **203**, 937–955.

Armstrong, R. L. (1988). Mesozoic and early Cenozoic magmatic evolution of the Canadian Cordillera. In: Burchfiel, B. C. & Suppe, J. (eds) *Processes in Continental Lithospheric Deformation. Geological Society of America, Special Papers* **218**, 55–92.

Armstrong, R. L. & Ward, P. (1991). Evolving geographic patterns of Cenozoic magmatism in the North American Cordillera: the temporal and spatial association of magmatism and metamorphic core complexes. *Journal of Geophysical Research* **96**, 13201–13224.

Armstrong, R. L., Taubeneck, W. H. & Hales, P. O. (1977). Rb–Sr and K–Ar geochronometry of Mesozoic granitic rocks and their Sr isotopic composition, Oregon, Washington, and Idaho. *Geological Society of America Bulletin* **88**, 397–411.

Bateman, P. C. (1992). *Plutonism in the central part of the Sierra Nevada batholith. US Geological Survey, Professional Papers* **1483**, 186 p.

Bickford, M. E., Chase, R. B., Nelson, B. K., Shuster, R. D. & Arruda, E. C. (1981). U–Pb studies of zircon cores and overgrowths, and monazite; implications for age and petrogenesis of the northeastern Idaho Batholith. *Journal of Geology* **89**, 433–457.

Boghossian, N. D., Patchett, P. J., Ross, G. M. & Gehrels, G. E. (1996). Nd isotopes and the source of sediments in the miogeocline of the Canadian Cordillera. *Journal of Geology* **104**, 259–277.

Bouvier, A., Vervoort, J. D. & Patchett, P. J. (2008). The Lu–Hf and Sm–Nd isotopic composition of CHUR: Constraints from unequilibrated chondrites and implications for the bulk composition of terrestrial planets. *Earth and Planetary Science Letters* **273**, 48–57.

Breitsprecher, K., Thorkelson, D. J., Groome, W. G. & Dostal, J. (2003). Geochemical confirmation of the Kula–Farallon slab window beneath the Pacific Northwest in Eocene time. *Geology* **31**, 351–354.

Brewer, R. A., Vervoort, J. D., Lewis, R. S., Gashnig, R. M. & Hart, G. L. (2008). New constraints on the extent of Paleoproterozoic and Archean basement in the northwest U.S. Cordillera. *EOS, Transactions, American Geophysical Union, Fall Meeting Supplement* **89**, Abstract T23C–2066.

Chase, R. B., Bickford, M. E. & Tripp, S. E. (1978). Rb–Sr and U–Pb isotopic studies of the northeastern Idaho Batholith and border zone. *Geological Society of America Bulletin* **89**, 1325–1334.

Clarke, C. B. (1990). The geochemistry of the Atlanta lobe of the Idaho batholith in the western United States Cordillera, PhD thesis, The Open University, Milton Keynes.

Coleman, D. S. & Glazner, A. F. (1997). The Sierra Crest magmatic event; rapid formation of juvenile crust during the Late Cretaceous in California. *International Geology Review* **39**, 768–787.

Constenius, K. N. (1996). Late Paleogene extensional collapse of the Cordilleran foreland fold and thrust belt. *Geological Society of America Bulletin* **108**, 20–39.

Criss, R. E. & Fleck, R. J. (1987). Petrogenesis, geochronology, and hydrothermal systems of the northern Idaho batholith and adjacent areas based on $^{18}O/^{16}O$, D/H, $^{87}Sr/^{86}Sr$, K–Ar, and $^{40}Ar/^{39}Ar$ studies. In: Vallier, T. L. & Brooks, H. C. (eds) *Geology of the Blue Mountains region of Oregon, Idaho, and Washington; the Idaho Batholith and its border zone US Geological Survey, Professional Papers* **1436**, 95–137.

Criss, R. E. & Fleck, R. J. (1990). Oxygen isotope map of the giant metamorphic–hydrothermal system around the northern part of the Idaho Batholith, U.S.A. *Applied Geochemistry* **5**, 641–655.

Criss, R. E. & Taylor, H. P., Jr (1983). An $^{18}O/^{16}O$ and D/ H study of Tertiary hydrothermal systems in the southern half of the Idaho Batholith. *Geological Society of America Bulletin* **94**, 640–663.

Davidson, J. P. & Arculus, R. J. (2005). The significance of Phanerozoic arc magmatism in generating continental crust. In: Brown, M. & Rushmer, T. (eds) *Evolution and Differentiation of the Continental Crust*. Cambridge: Cambridge University Press, pp. 135–172.

DeCelles, P. G. (2004). Late Jurassic to Eocene evolution of the Cordilleran thrust belt and foreland basin system, western U.S.A. *American Journal of Science* **304**, 105–168.

DeCelles, P. G., Ducea, M. N., Kapp, P. & Zandt, G. (2009). Cyclicity in Cordilleran orogenic systems. *Nature, Geoscience* **2**, 251–257.

Doe, B. R. & Sanford, R. F. (1995). Lead-isotope characteristics of ore systems in central Idaho. In: Worl, R. G., Link, P. K., Winkler, G. R. & Johnson, K. M. (eds) *Geology and Mineral Resources of the Hailey 1° × 2° quadrangle and the western part of the Idaho Falls 1° × 2° quadrangle, Idaho. US Geological Survey, Bulletin* **2064M**, M1–M29.

Doughty, P. T. & Chamberlain, K. R. (1996). Salmon River Arch revisited: new evidence for 1370 Ma rifting near the end of deposition in the Middle Proterozoic Belt Basin. *Canadian Journal of Earth Sciences* **33**, 1037–1052.

Doughty, P. T. & Chamberlain, K. R. (2007). Age of Paleoproterozoic basement and related rocks in the Clearwater complex, northern Idaho, U.S.A. In: Link, P. K. & Lewis, R. S. (eds) *Proterozoic Geology of Western North America and Siberia*. Tulsa, OK: SEPM, pp. 9–36.

Doughty, P. T., Price, R. A. & Parrish, R. R. (1998). Geology and U–Pb geochronology of Archean basement and Proterozoic cover in the Priest River complex, northwestern United States, and their implications for Cordilleran structure and Precambrian continent reconstructions. *Canadian Journal of Earth Sciences* **35**, 39–54.

Doughty, P. T., Chamberlain, K. R., Foster, D. A. & Sha, G. S. (2007). Structural, metamorphic, and geochronological constraints on the origin of the Clearwater core complex, northern Idaho. In: Sears, J. W., Harms, T. A. & Evenchick, C. A. (eds) *Whence the Mountains? Inquiries into the Evolution of Orogenic Systems: A Volume in Honor of Raymond A. Price. Geological Society of America, Special Papers* **433**, 211–241.

Ducea, M. (2001). The California arc: thick granitic batholiths, eclogitic residues, lithospheric-scale thrusting, and magmatic flare-ups. *GSA Today* **11**, 4–10.

Ducea, M. N. & Barton, M. D. (2007). Igniting flare-up events in Cordilleran arcs. *Geology* **35**, 1047–1050.

Dudas, F., Carlson, R. W. & Eggler, D. H. (1987). Regional Middle Proterozoic enrichment of the subcontinental mantle source of igneous rocks from central Montana. *Geology* **15**, 22–25.

Duke, G. I. (2005). Geochemistry and geochronology of Paleocene–Eocene alkalic igneous rocks, northern Black Hills, South Dakota and Wyoming. PhD thesis, South Dakota School of Mines and Technology, Rapid City.

Duke, G. I. (2009). Black Hills–Alberta carbonatite–kimberlite linear trend: slab edge at depth? *Tectonophysics* **464**, 186–194.

Durk, K. M. (2007). Geochronology of part of the Wildhorse gneiss complex, Pioneer Mountains, Custer County, Idaho. BS thesis. Idaho State University, Pocatello.

Dye, J. H., Schmitz, M. D. & Crowley, J. L. (2009). Metamorphic evolution of the Houes Mountain gneiss complex, southwest Idaho. *Geological Society of America, Abstracts with Programs* **41**, 692.

Ellam, R. M. & Hawkesworth, C. J. (1988). Is average continental crust generated at subduction zones? *Geology* **16**, 314–317.

Engebretson, D. C., Cox, A. & Gordon, R. G. (1984). Relative motions between oceanic plates of the Pacific Basin. *Journal of Geophysical Research* **89**, 10291–10310.

Feeley, T. C. (2003). Origin and tectonic implications of across-strike geochemical variations in the Eocene Absaroka Volcanic Province, United States. *Journal of Geology* **111**, 329–346.

Fleck, R. J. (1990). Neodymium, strontium, and trace-element evidence of crustal anatexis and magma mixing in the Idaho Batholith. In: Anderson, J. L. (ed.) *The Nature and Origin of Cordilleran Magmatism. Geological Society of America, Memoirs* **174**, 359–373.

Fleck, R. J. & Criss, R. E. (1985). Strontium and oxygen isotopic variations in Mesozoic and Tertiary plutons of central Idaho. *Contributions to Mineralogy and Petrology* **90**, 291–308.

Fleck, R. J. & Criss, R. E. (2007). Location, age, and tectonic significance of the Western Idaho suture zone. In: Kuntz, M. A. & Snee, L. W. (eds) *Geological studies of the Salmon River suture zone and adjoining areas, west–central Idaho and eastern Oregon. US Geological Survey, Professional Papers* **1738**, 15–50.

Fleck, R. J., Criss, R. E., Eaton, G. F., Cleland, R. W., Wavra, C. S. & Bond, W. D. (2002). Age and origin of base and precious metal veins of the Coeur D'Alene mining district, Idaho. *Economic Geology* **97**, 23–42.

Foster, D. A. & Fanning, C. M. (1997). Geochronology of the northern Idaho Batholith and the Bitterroot metamorphic core complex; magmatism preceding and contemporaneous with extension. *Geological Society of America Bulletin* **109**, 379–394.

Foster, D. A. & Hyndman, D. W. (1990). Magma mixing and mingling between synplutonic mafic dikes and granite in the Idaho–Bitterroot Batholith. In: Anderson, J. L. (ed.) *The Nature and Origin of Cordilleran Magmatism. Geological Society of America, Memoirs* **174**, 347–358.

Foster, D. A., Schafer, C., Fanning, C. M. & Hyndman, D. W. (2001). Relationships between crustal partial melting, plutonism, orogeny, and exhumation; Idaho–Bitterroot Batholith. *Tectonophysics* **342**, 313–350.

Foster, D. A., Mueller, P. A., Mogk, D. W., Wooden, J. L. & Vogl, J. J. (2006). Proterozoic evolution of the western margin of the Wyoming craton: implications for the tectonic and magmatic evolution of the northern Rocky Mountains. *Canadian Journal of Earth Sciences* **43**, 1601–1619.

Friedman, R. M., Mahoney, J. B. & Cui, Y. (1995). Magmatic evolution of the southern Coast Belt: constraints from Nd–Sr isotopic systematics and geochronology of the southern Coast Plutonic Complex. *Canadian Journal of Earth Sciences* **32**, 1681–1698.

Frost, B. R., Barnes, C. G., Collins, W. J., Arculus, R. J., Ellis, D. J. & Frost, C. D. (2001). A Geochemical Classification for Granitic Rocks. *Journal of Petrology* **42**, 2033–2048.

Frost, C. D. & Winston, D. (1987). Nd isotope systematics of coarse- and fine-grained sediments: examples from the Middle Proterozoic Belt–Purcell Supergroup. *Journal of Geology* **95**, 309–327.

Galer, S. J. G. & Abouchami, W. (1998). Practical application of lead triple spiking for correction of instrumental mass discrimination. *Mineralogical Magazine* **62A**, 491–492.

Gaschnig, R. M., Vervoort, J. D., Lewis, R. S. & Dufrane, S. A. (2008*a*). Utilizing U–Pb geochronology of inherited zircon in the Atlanta lobe of the Idaho batholith as a probe of the deep crust in southern Idaho: a progress report. *Northwest Geology* **37**, 101–110.

Gaschnig, R. M., Vervoort, J. D., Lewis, R. S., Valley, J. W., King, E. M., Kozdon, R., Ushikubo, T., Dufrane, S. A., Hart, G., Knaack, C. & McClelland, W. (2008*b*). Coupled Hf–O isotopic perspective on 50 million years of magmatism in the Idaho batholith. *EOS, Transactions, American Geophysical Union, Fall Meeting Supplement* **89**, Abstract V21C–2119.

Gaschnig, R. M., Vervoort, J. D., Lewis, R. S. & McClelland, W. C. (2010). Migrating magmatism in the northern US Cordillera: *in situ* U–Pb geochronology of the Idaho batholith. *Contributions to Mineralogy and Petrology* **159**, 863–883.

Gaschnig, R. M., Vervoort, J. D., Lewis, R. S. & Tikoff, B. (in preparation). Insights into Precambrian basement architecture in the northern U.S. Cordillera provided by inherited zircons from the Idaho batholith. *Geological Society of America Bulletin*.

Giorgis, S., McClelland, W., Fayon, A., Singer, B. S. & Tikoff, B. (2008). Timing of deformation and exhumation in the western Idaho shear zone, McCall, Idaho. *Geological Society of America Bulletin* **120**, 1119–1133.

Goodge, J. W. & Vervoort, J. D. (2006). Origin of Mesoproterozoic A-type granites in Laurentia: Hf isotope evidence. *Earth and Planetary Science Letters* **243**, 711–731.

Gray, W., Glazner, A. F., Coleman, D. S. & Bartley, J. M. (2008). Long-term geochemical variability of the Late Cretaceous Tuolumne Intrusive Suite, central Sierra Nevada, California. In: Annen, C. & Zellmer, G. F. (eds) *Dynamics of Crust Transfer, Storage, and Differentiation. Geological Society, London, Special Publications* **304**, 183–201.

Gromet, P. & Silver, L. T. (1987). REE variations across the Peninsular Ranges batholith: implications for batholithic petrogenesis and crustal growth in magmatic arcs. *Journal of Petrology* **28**, 75–125.

Haeussler, P. J., Bradley, D. C., Wells, R. E. & Miller, M. L. (2003). Life and death of the Resurrection plate: Evidence for its existence and subduction in the northeastern Pacific in Paleocene and Eocene time. *Geological Society of America Bulletin* **115**, 867–880.

Haggart, J. W., Enkin, R. J. & Monger, J. W. H. (2006). Strengths and limitations of paleogeographic methods in assessing large-scale displacements within the North American Cordillera. In: Haggart, J. W., Enkin, R. J. & Monger, J. W. H. (eds) *Paleogeography of the North American Cordillera; Evidence for and against Large-scale Displacements. Geological Association of Canada, Special Papers* **46**, 1–11.

Hildreth, W. & Moorbath, S. (1988). Crustal contributions to arc magmatism in the Andes of central Chile. *Contributions to Mineralogy and Petrology* **98**, 455–589.

House, M. A., Hodges, K. V. & Bowring, S. A. (1997). Petrological and geochronological constraints on regional metamorphism along the northern border of the Bitterroot batholith. *Journal of Metamorphic Geology* **15**, 753–764.

Humphreys, E. D. (1995). Post-Laramide removal of the Farallon slab, western United States. *Geology* **23**, 987–990.

Hyndman, D. W. (1983). The Idaho Batholith and associated plutons, Idaho and western Montana. In: Roddick, J. A. (ed.) *Circum-Pacific Plutonic Terranes. Geological Society of America, Memoirs* **159**, 213–240.

Hyndman, D. W. (1984). A petrographic and chemical section through the northern Idaho Batholith. *Journal of Geology* **92**, 83–102.

Hyndman, D. W. & Foster, D. A. (1988). The role of tonalites and mafic dikes in the generation of the Idaho Batholith. *Journal of Geology* **96**, 31–46.

Hyndman, D. W., Alt, D. & Sears, J. W. (1988). Post-Archean metamorphic and tectonic evolution of western Montana and northern Idaho. In: Ernst, W. G. (ed.) *Metamorphism and Crustal Evolution of the Western United States*. Englewood Cliffs, NJ: Prentice Hall, pp. 332–361.

Irving, E. (1985). Tectonics: whence British Columbia? *Nature* **314**, 673–674.

Johnson, D. M., Hooper, P. R. & Conrey, R. M. (1999). XRF analysis of rocks and minerals for major and trace elements on a single low dilution Li-tetraborate fused bead. *Advances in X-ray Analysis* **41**, 843–867.

Kelemen, P. B., Hanghoj, K. & Greene, A. R. (2003). One view of the geochemistry of subduction-related magmatic arcs, with an emphasis on primitive andesite and lower crust. In: Rudnick, R. L. (ed.) *Treatise on Geochemistry: The Crust*. Oxford: Elsevier–Pergamon, pp. 593–659.

Kemp, A. I. S., Hawkesworth, C. J., Collins, W. J., Gray, C. M. & Blevin, P. L. (2009). Isotopic evidence for rapid continental growth in an extensional accretionary orogen: The Tasmanides, eastern Australia. *Earth and Planetary Science Letters* **284**, 455–466.

Kiilsgaard, T. H. & Lewis, R. S. (1985). Plutonic rocks of Cretaceous age and faults in the Atlanta Lobe of the Idaho Batholith, Challis Quadrangle. In: McIntyre, D. H. (ed.) *Symposium on the Geology and Mineral Deposits of the Challis 1 degrees × 2 degrees Quadrangle, Idaho. US Geological Survey, Bulletin* **1658**, 29–42.

King, E. M. & Valley, J. W. (2001). The source, magmatic contamination, and alteration of the Idaho Batholith. *Contributions to Mineralogy and Petrology* **142**, 72–88.

King, E. M., Beard, B. L. & Valley, J. W. (2007). Strontium and oxygen isotopic evidence for strike/slip movement of accreted terranes in the Idaho Batholith. *Lithos* **96**, 387–401.

Knaack, C., Cornelius, S. & Hooper, P. R. (1994). Trace element analysis of rocks and minerals by ICP-MS. Open File Report, Department of Geology. Pullman: Washington State University.

Larson, P. B. & Geist, D. J. (1995). On the origin of low-^{18}O magmas: evidence from the Casto pluton, Idaho. *Geology* **23**, 909–912.

Lee, C.-T. A., Morton, D. M., Kistler, R. W. & Baird, A. K. (2007). Petrology and tectonics of Phanerozoic continent formation: From

island arcs to accretion and continental arc magmatism. *Earth and Planetary Science Letters* **263**, 370–387.

Lee, R. G. (2004). The geochemistry, stable isotopic composition, and U–Pb geochronology of tonalite trondhjemites within the accreted terrane, near Greer, north–central Idaho. MS thesis, Washington State University, Pullman.

Leeman, W. P., Menzies, M. A., Matty, D. J. & Embree, G. F. (1985). Strontium, neodymium and lead isotopic compositions of deep crustal xenoliths from the Snake River Plain: evidence for Archean basement. *Earth and Planetary Science Letters* **75**, 354–368.

Lewis, R. S. & Frost, T. P. (2005). Major oxide and trace element analyses for igneous and metamorphic rock samples from northern and central Idaho. *Idaho Geological Survey—Digital Analytical Data* **2.**

Lewis, R. S. & Kiilsgaard, T. H. (1991). Eocene plutonic rocks in south central Idaho. *Journal of Geophysical Research* **96**, 13295–13311.

Lewis, R. S., Kiilsgaard, T. H., Bennett, E. H. & Hall, W. E. (1987). Lithologic and chemical characteristics of the central and southeastern part of the southern lobe of the Idaho Batholith. In: Vallier, T. L. & Brooks, H. C. (eds) *Geology of the Blue Mountains region of Oregon, Idaho, and Washington: the Idaho Batholith and its border zone. US Geological Survey, Professional Papers* **1436**, 171–196.

Lewis, R. S., Burmester, R. F., Kauffman, J. D., Breckenridge, R. M., Schmidt, K. L., McFaddan, M. D. & Myers, P. E. (2007*a*). Geologic map of the Kooskia 30 × 60 minute quadrangle, Idaho. *Idaho Geological Survey Digital Web Map* **93**, 1:100 000.

Lewis, R. S., Vervoort, J. D., Burmester, R. F., McClelland, W. C. & Chang, Z. (2007*b*). Geochronological constraints on Mesoproterozoic and Neoproterozoic(?) high-grade metasedimentary rocks of north–central Idaho, U.S.A. In: Link, P. K. & Lewis, R. S. (eds) *Proterozoic Geology of Western North American and Siberia*. Tulsa: SEPM, pp. 37–54.

Link, P. K., Fanning, C. M., Lund, K. I. & Aleinikoff, J. N. (2007). Detrital-zircon populations and provenance of Mesoproterozoic strata of east–central Idaho, U.S.A.: correlation with the Belt Supergroup of southwest Montana. In: Link, P. K. & Lewis, R. S. (eds) *Proterozoic Geology of Western North America and Siberia*. Tulsa: SEPM, pp. 101–128.

Lund, K. & Snee, L. W. (1988). Metamorphism, structural development, and age of the continental–island arc juncture in west–central Idaho. In: Ernst, W. G. (ed.) *Metamorphism and Crustal Evolution, Western Conterminous United States*. Englewood Cliffs, NJ: Prentice Hall, pp. 296–331.

Lund, K., Aleinikoff, J. N., Evans, K. V. & Fanning, C. M. (2003). SHRIMP U–Pb geochronology of Neoproterozoic Windermere Supergroup, central Idaho: implications for rifting of western Laurentia and synchroneity of Sturtian glacial deposits. *Geological Society of America Bulletin* **115**, 349–372.

Lund, K., Aleinikoff, J. N., Yacob, E. Y., Unruh, D. M. & Fanning, C. M. (2008). Coolwater culmination: sensitive high-resolution ion microprobe (SHRIMP) U–Pb and isotopic evidence for continental delamination in the Syringa Embayment, Salmon River suture, Idaho. *Tectonics* **27**, TC2009.

Lund, K., Aleinikoff, J. N., Evans, K. V., duBray, E. A., Dewitt, E. H. & Unruh, D. M. (2010). SHRIMP U–Pb dating of recurrent Cryogenian and Late Cambrian–Early Ordovician alkalic magmatism in central Idaho: implications for Rodinian rift tectonics. *Geological Society of America Bulletin* **122**, 430–453.

Madsen, J. K., Thorkelson, D. J., Friedman, R. M. & Marshall, D. D. (2006). Cenozoic to Recent plate configurations in the Pacific Basin: ridge subduction and slab window magmatism in western North America. *Geosphere* **2**, 11–34.

Mahoney, J. B., Tikoff, B., Maxson, J. & Haugerud, R. A. (2000). Terrane accretion along the western Cordilleran margin: Constraints on timing and displacement. *GSA Today* **10**, 11–13.

Manduca, C. A., Silver, L. T. & Taylor, H. P., Jr (1992). $^{87}Sr/^{86}Sr$ and $^{18}O/^{16}O$ isotopic systematics and geochemistry of granitoid plutons across a steeply-dipping boundary between contrasting lithospheric blocks in western Idaho. *Contributions to Mineralogy and Petrology* **109**, 355–372.

Manduca, C. A., Kuntz, M. A. & Silver, L. T. (1993). Emplacement and deformation history of the western margin of the Idaho Batholith near McCall, Idaho; influence of a major terrane boundary. *Geological Society of America Bulletin* **105**, 749–765.

Maxson, J. & Tikoff, B. (1996). Hit-and-run collision model for the Laramide orogeny, western United States. *Geology* **24**, 968–972.

McClelland, W. C. & Oldow, J. S. (2007). Late Cretaceous truncation of the western Idaho shear zone in the central North American Cordillera. *Geology* **35**, 723–726.

McClelland, W. C., Tikoff, B. & Manduca, C. A. (2000). Two-phase evolution of accretionary margins: examples from the North American Cordillera. *Tectonophysics* **326**, 37–55.

McDonough, W. F. & Sun, S.-S. (1995). Composition of the Earth. *Chemical Geology* **120**, 223–253.

McKervey, A. (1998). The petrogenesis of the Eocene Challis Volcanic Group, Idaho, western U.S.A. PhD thesis. The Open University, Milton Keynes.

Mitchell, T. A. (1997). Petrology, geochemistry, and petrogenesis of the Eocene Big Smoky Creek Stock, south–central Idaho. MS thesis, Washington State University, Pullman.

Motzer, W. E. (1985). Tertiary epizonal plutonic rocks of the Selway–Bitterroot Wilderness, Idaho County, Idaho. PhD thesis, University of Idaho, Moscow.

Moyen, J.-F. (2009). High Sr/Y and La/Yb ratios: The meaning of the 'adakitic signature'. *Lithos* **112**, 556–574.

Mueller, P. A., Shuster, R. D., D'Arcy, K. A., Heatherington, A. L., Nutman, A. P. & Williams, I. S. (1995). Source of the northeastern Idaho Batholith; isotopic evidence for a Paleoproterozoic terrane in the Northwestern U.S. *Journal of Geology* **103**, 63–72.

Münker, C., Weyer, S., Scherer, E. & Mezger, K. (2001). Separation of high field strength elements (Nb, Ta, Zr, Hf) and Lu from rock samples for MC-ICPMS measurements. *Geochemistry, Geophysics, Geosystems* **2**, 2001GC000183.

Murphy, J. J. (2007). Kinematics, partitioning and the relationship between velocity and strain in shear zones. PhD thesis, Washington State University, Pullman.

Norman, M. D. & Leeman, W. P. (1989). Geochemical evolution of Cenozoic–Cretaceous magmatism and its relation to tectonic setting, southwestern Idaho, U.S.A. *Earth and Planetary Science Letters* **94**, 78–96.

Norman, M. D. & Mertzman, S. A. (1991). Petrogenesis of Challis Volcanics from central and southwestern Idaho: trace element and Pb isotopic evidence. *Journal of Geophysical Research* **96**, 13279–13293.

Norman, M. D., Leeman, W. P. & Mertzman, S. A. (1992). Granites and rhyolites from the northwestern U.S.A.: temporal variation in magmatic processes and relations to tectonic setting. *Transactions of the Royal Society of Edinburgh: Earth Sciences* **83**, 71–81.

O'Brien, H. E., Irving, A. J., McCallum, I. S. & Thirlwall, M. F. (1995). Strontium, neodymium, and lead isotopic evidence for the interaction of post-subduction asthenospheric potassic mafic magmas of the Highwood Mountains, Montana, USA, with ancient Wyoming craton lithospheric mantle. *Geochimica et Cosmochimica Acta* **59**, 4539–4556.

Ortega-Rivera, A. (2003). Geochronological constraints on the tectonic history of the Peninsular Ranges batholith of Alta and Baja

California; tectonic implications for western Mexico. In: Johnson, S. E., Paterson, S. R., Fletcher, J. M., Girty, G. H., Kimbrough, D. L. & Martin-Barajas, A. (eds) *Tectonic Evolution of Northwestern Mexico and the Southwestern USA. Geological Society of America, Special Papers* **374**, 297–335.

Ortega-Rivera, A., Farrar, E., Hanes, J. A., Archibald, D. A., Gastil, R. G., Kimbrough, D. L., Zentilli, M., Lopez-Martinez, M., Feraud, G. & Ruffet, G. (1997). Chronological constraints on the thermal and tilting history of the Sierra San Pedro Martir pluton, Baja California, Mexico, from U/Pb, $^{40}Ar/^{39}Ar$, and fission-track geochronology. *Geological Society of America Bulletin* **109**, 728–745.

Panneerselvam, K., McFarlane, A. W. & Salters, V. J. M. (2006). Provenance of ore metals in base and precious metal deposits of central Idaho as inferred from lead isotopes. *Economic Geology* **101**, 1063–1077.

Patiño Douce, A. E. (1999). What do experiments tell us about the relative contributions of crust and mantle to the origin of granitic magmas? In: Castro, A., Fernandez, C. & Vigneresse, J. L. (eds) *Understanding Granites: Integrating New and Classical Techniques Geological Society, London. Special Publications* **158**, 55–75

Patiño Douce, A. E. & Beard, J. S. (1995). Dehydration-melting of biotite gneiss and quartz amphibolite from 3 to 15 kbar. *Journal of Petrology* **36**, 707–738.

Pearce, J. A. (1982). Trace element characteristics of lavas from destructive plate boundaries. In: Thorpe, R. S. (ed.) *Andesites: Orogenic Andesites and Related Rocks*. Chichester: Wiley, pp. 525–548.

Petford, N. & Atherton, M. P. (1996). Na-rich partial melts from newly underplated basaltic crust: the Cordillera Blanca batholith, Peru. *Journal of Petrology* **37**, 1491–1521.

Reppe, T. H. (1997). Geology, geochemistry, and petrogenesis of the Eocene Prairie Creek Stock, Smoky Mountains, Blaine and Camas Counties, Idaho. MS thesis, Washington State University, Pullman.

Robertson, M. C. (1997). Geochemistry and petrogenesis of the Eocene Boulder Mountain Stock, central Idaho. MS thesis, Washington State University, Pullman.

Ross, G. M. & Villeneuve, M. (2003). Provenance of the Mesoproterozoic (1·45 Ga) Belt basin (western North America): Another piece in the pre-Rodinia paleogeographic puzzle. *Geological Society of America Bulletin* **115**, 1191–1217.

Rudnick, R. (1995). Making continental crust. *Nature* **378**, 571–578.

Russell, C. W. & Gabites, J. (2005). Elevated $^{87}Sr/^{86}Sr$ ratios from mafic intrusions in the Atlanta lobe of the Idaho batholith. *Idaho Geological Survey, Technical Report*, **05–01**.

Saleeby, J. B., Ducea, M. N. & Clemens-Knott, D. (2003). Production and loss of high-density batholithic root, southern Sierra Nevada, California. *Tectonics* **22**, 1064.

Saleeby, J. B., Ducea, M. N., Busby, C. J., Nadin, E. S. & Wetmore, P. H. (2008). Chronology of pluton emplacement and regional deformation in the southern Sierra Nevada batholith, California. In: Wright, J. E. & Shervais, J. W. (eds) *Ophiolites, Arcs, and Batholiths: a Tribute to Cliff Hopson. Geological Society of America, Special Papers* **438**, 397–427.

Schmidt, K. L., Lewis, R. S., Gaschnig, R. M. & Vervoort, J. D. (2009). Testing hypotheses on the origin of the Syringa embayment in the Salmon River suture zone, western Idaho, USA. *Geological Society of America, Abstracts with Programs* **41**, 223.

Shuster, R. D. & Bickford, M. E. (1985). Chemical and isotopic evidence for the petrogenesis of the northeastern Idaho Batholith. *Journal of Geology* **93**, 727–742.

Silverberg, D. S. (1990). The tectonic evolution of the Pioneer metamorphic core complex, south–central Idaho. PhD thesis, Massachusetts Institute of Technology, Cambridge.

Sims, P. K., Lund, K. & Anderson, E. (2005). Precambrian crystalline basement map of Idaho—an interpretation of aeromagnetic anomalies. *US Geological Survey Scientific Investigation Map* **2884**, 1:1 000 000.

Skjerlie, K. P. & Patiño Douce, A. E. (1995). Anatexis of interlayered amphibolite and pelite at 10 kbar: effect of diffusion of major components on phase relations and melt fraction. *Contributions to Mineralogy and Petrology* **122**, 62–78.

Skjerlie, K. P., Patiño Douce, A. E. & Johnston, A. D. (1993). Fluid absent melting of a layered crustal protolith: implications for the generation of anatectic granites. *Contributions to Mineralogy and Petrology* **114**, 365–378.

Snee, L. W., Davidson, G. F. & Unruh, D. M. (2007). Geological, geochemical, and 40Ar/39Ar and U–Pb thermochronological constraints for the tectonic development of the Salmon River suture zone near Orofino, Idaho. In: Kuntz, M. A. & Snee, L. W. (eds) *Geological studies of the Salmon River suture zone and adjoining areas, west–central Idaho and eastern Oregon. US Geological Survey, Professional Papers* **1738**, 51–94.

Stock, J. & Molnar, P. (1988). Uncertainties and implications of the Late Cretaceous and Tertiary position of North America relative to the Farallon, Kula, and Pacific plates. *Tectonics* **7**, 1339–1384.

Todd, V. R. & Shaw, S. E. (1985). S-type granitoids and an I–S line in the Peninsular Ranges batholith, southern California. *Geology* **13**, 231–233.

Toth, M. I. (1987). Petrology and origin of the Bitterroot Lobe of the Idaho Batholith. In: Vallier, T. L. & Brooks, H. C. (eds) *Geology of the Blue Mountains region of Oregon, Idaho, and Washington; the Idaho Batholith and its border zone. US Geological Survey, Professional Papers* **1436**, 9–35.

Toth, M. I. & Stacey, J. S. (1992). Constraints on the formation of the Bitterroot lobe of the Idaho batholith, Idaho and Montana, from U–Pb zircon geochronology and feldspar Pb isotopic data. *US Geological Survey Bulletin* **2008**, 14.

Truschel, J. P. (1996). Petrogenesis of the Fine Gold intrusive suite, Sierra Nevada Batholith, California. MS thesis, California State University, Northridge.

Umhoefer, P. J. & Blakey, R. (2006). Moderate (1600 km) northward translation of Baja British Columbia from southern California: An attempt at reconciliation of paleomagnetism and geology. In: Haggart, J. W., Enkin, R. J. & Monger, J. W. H. (eds) *Paleogeography of the North American Cordillera: evidence for and against large-scale displacements. Geological Association of Canada, Special Papers* **46**, 307–329.

Unruh, D. M., Lund, K., Snee, L. W. & Kuntz, M. A. (2008). Uranium–lead zircon ages and Sr, Nd, and Pb isotope geochemistry of selected plutonic rocks from western Idaho. *US Geological Survey, Open-File Report* , 2008–1142, 42 pp.

Van Buer, N. J. & Miller, E. L. (2010). Sahwave Batholith, NW Nevada: Cretaceous arc flare-up in a basinal terrane. *Lithosphere* **2**, 423–446.

Vervoort, J. D. & Blichert-Toft, J. (1999). Evolution of the depleted mantle: Hf isotope evidence from juvenile rocks through time. *Geochimica et Cosmochimica Acta* **63**, 533–556.

Vervoort, J. D., Patchett, P. J., Soderlund, U. & Baker, M. (2004). Isotopic composition of Yb and the determination of Lu concentrations and Lu/Hf ratios by isotope dilution using MC-ICPMS. *Geochemistry, Geophysics, Geosystems* **5**, Q11002.

Vervoort, J. D., Zirakparvar, N. A., Lewis, R. S. & Burmester, R. F. (2007). Evidence for recurrent Paleoproterozoic and Mesoproterozoic magmatism and metamorphism in the Boehls Butte–Clarkia area, north–central Idaho, U.S.A. *Geological Society of America, Abstracts with Programs* **39**, 245.

Watkins, J., Clemens, J. & Treloar, P. (2007). Archaean TTGs as sources of younger granitic magmas: melting of sodic metatonalites at 0·6–1·2 GPa. *Contributions to Mineralogy and Petrology* **154**, 91–110.

Wells, M. L., Hoisch, T. D., Cruz-Uribe, A. M. & Vervoort, J. D. (2009). Geodynamics of synconvergent extension and tectonic mode switching: constraints from the Sevier–Laramide orogen. *Geological Society of America, Abstracts with Programs* **41**, 588.

White, W. M., Albarède, F. & Télouk, P. (2000). High-precision analysis of Pb isotope ratios by multi-collector ICP-MS. *Chemical Geology* **167**, 257–270.

Wolf, D. E., Leeman, W. P. & Vervoort, J. D. (2005). U–Pb zircon geochronology of crustal xenoliths confirms presence of Archean basement beneath the central and eastern Snake River Plain. *Geological Society of America, Abstracts with Programs* **37**, 60.

Woodhead, J., Hergt, J., Shelley, M., Eggins, S. & Kemp, R. (2004). Zircon Hf-isotope analysis with an excimer laser, depth profiling, ablation of complex geometries, and concomitant age estimation. *Chemical Geology* **209**, 121–135.

Wyld, S. J., Umhoefer, P. J. & Wright, J. E. (2006). Reconstructing northern Cordillera terranes along known Cretaceous and Cenozoic strike-slip faults: implications for the Baja British Columbia hypothesis and other models. In: Haggart, J. W., Enkin, R. J. & Monger, J. W. H. (eds) *Paleogeography of the North American Cordillera: Evidence for and against Large-scale Displacements. Geological Association of Canada, Special Papers* **46**, 277–298.